Limnol. Oceanogr., 58(1), 2013, 325–342

doi:10.4319/lo.2013.58.1.0325

The marine inorganic carbon system along the Gulf of Mexico and Atlantic coasts of the United States: Insights from a transregional coastal carbon study

Zhaohui Aleck Wang,[a,*] Rik Wanninkhof,[b] Wei-Jun Cai,[c] Robert H. Byrne,[d] Xinping Hu,[e] Tsung-Hung Peng,[b] and Wei-Jen Huang [c]

[a] Marine Chemistry and Geochemistry, Woods Hole Oceanographic Institution, Woods Hole, Massachusetts
[b] National Oceanic and Atmospheric Administration Atlantic Oceanographic and Meteorological Laboratory, Miami, Florida
[c] Department of Marine Sciences, University of Georgia, Athens, Georgia
[d] College of Marine Science, University of South Florida, St. Petersburg, Florida
[e] Department of Physical and Environmental Sciences, Texas A&M University - Corpus Christi, Corpus Christi, Texas

Abstract

Distributions of total alkalinity (TA), dissolved inorganic carbon (DIC), and other parameters relevant to the marine inorganic carbon system were investigated in shelf and adjacent ocean waters during a U.S. Gulf of Mexico and East Coast Carbon cruise in July–August 2007. TA exhibited near-conservative behavior with respect to salinity. Shelf concentrations were generally high in southern waters (Gulf of Mexico and East Florida) and decreased northward from Georgia to the Gulf of Maine. DIC was less variable geographically and exhibited strongly nonconservative behavior. As a result, the ratio of TA to DIC generally decreased northward. The spatial patterns of other CO_2 system parameters closely followed those of the TA : DIC ratio. All sampled shelf waters were supersaturated with respect to aragonite (saturation state $\Omega_A > 1$). The most intensely buffered and supersaturated waters ($\Omega_A > 5.0$) were in northern Gulf of Mexico river-plume waters; the least intensely buffered and least supersaturated waters ($\Omega_A < 1.3$) were in the deep Gulf of Maine. Due to their relatively low pH, Ω_A, and buffer intensity, waters of the northeastern U.S. shelves may be more susceptible to acidification pressures than are their southern counterparts. In the Mid-Atlantic Bight, alongshore mixing tended to increase DIC concentrations southward, but this effect was largely offset by the opposing effects of biogeochemical processing. In the Gulf of Mexico, downstream increases in Loop Current DIC suggested significant contributions from shelf and gulf waters, estimated at 9.1×10^9 mol C d^{-1}. Off the southeastern U.S., along-flow chemical changes in the Florida Current were dominated by mixing associated with North Atlantic subtropical recirculation.

The world's continental shelves absorb on the order of 0.25–0.36 Pg C yr^{-1} from the atmosphere (Chen and Borges 2009), which is equivalent to ~ 16–23% of the net annual open-ocean CO_2 uptake (Takahashi et al. 2009). Substantially less information is available regarding other inorganic carbon fluxes, such as shelf–ocean exchanges and wetland inputs, which may be at least as important as air–sea CO_2 fluxes in shelf and global carbon budgets (Bouillon et al. 2008; Cai 2011). Large amounts of dissolved inorganic carbon (DIC) may be exported from shelves by 'continental shelf pump' mechanisms, whereby strong solubility and biological pumps encourage uptake of atmospheric CO_2 on the shelf, resulting in carbon-enriched waters that subsequently outflow to the open ocean (Tsunogai et al. 1999; Thomas et al. 2004). DIC export may also originate from the inner shelves, where terrestrial organic carbon oxidation is extensive (Hopkinson and Smith 2005). Recent global mass balance estimates (Chen and Borges 2009) suggest, however, that even with these export mechanisms, continental shelves may experience a net import of open-ocean DIC and nutrients that support excess (net) shelf organic carbon production. Uncertainties regarding shelf inorganic carbon fluxes, including air–sea CO_2 fluxes, are currently large, even for relatively well-studied shelf regions (Hofmann et al. 2011). Comprehensive observational programs are required to understand the carbon dynamics of coastal systems and the effects of many ecologically significant and societally relevant coastal processes (e.g., coastal acidification; Feely et al. 2008; Bates and Mathis 2009; Hauri et al. 2009). The large temporal and spatial variability of shelf environments presents a special challenge in this undertaking.

This study focuses on inorganic carbon biogeochemistry in the coastal waters of the eastern United States (Atlantic and Gulf of Mexico). These waters constitute a western ocean-boundary margin that encompasses tropical to temperate waters. This continental shelf is traditionally demarcated into six areas (Fig. 1): northern Gulf of Mexico (nGMx), West Florida Shelf (WFLS), East Florida Shelf (EFLS), South Atlantic Bight (SAB), Mid-Atlantic Bight (MAB), and Gulf of Maine (GoME). The southern portion, from nGMx to SAB, is bounded by the Loop Current–Florida Current–Gulf Stream system, which flows through the Gulf of Mexico and the Straits of Florida, then northward along the shelf break of the southeastern U.S. before being deflected into the North Atlantic Ocean off Cape Hatteras, North Carolina (Leaman et al. 1989). The GoME and MAB regions, in contrast, are bordered by a shelf-break front that separates fresh, generally southward-flowing shelf water from salty slope water frequently influenced by Gulf Stream meanders (Lozier and Gawarkiewicz 2001).

Previous observational studies of the inorganic carbon system along the U.S. East Coast have been primarily

* Corresponding author: zawang@whoi.edu

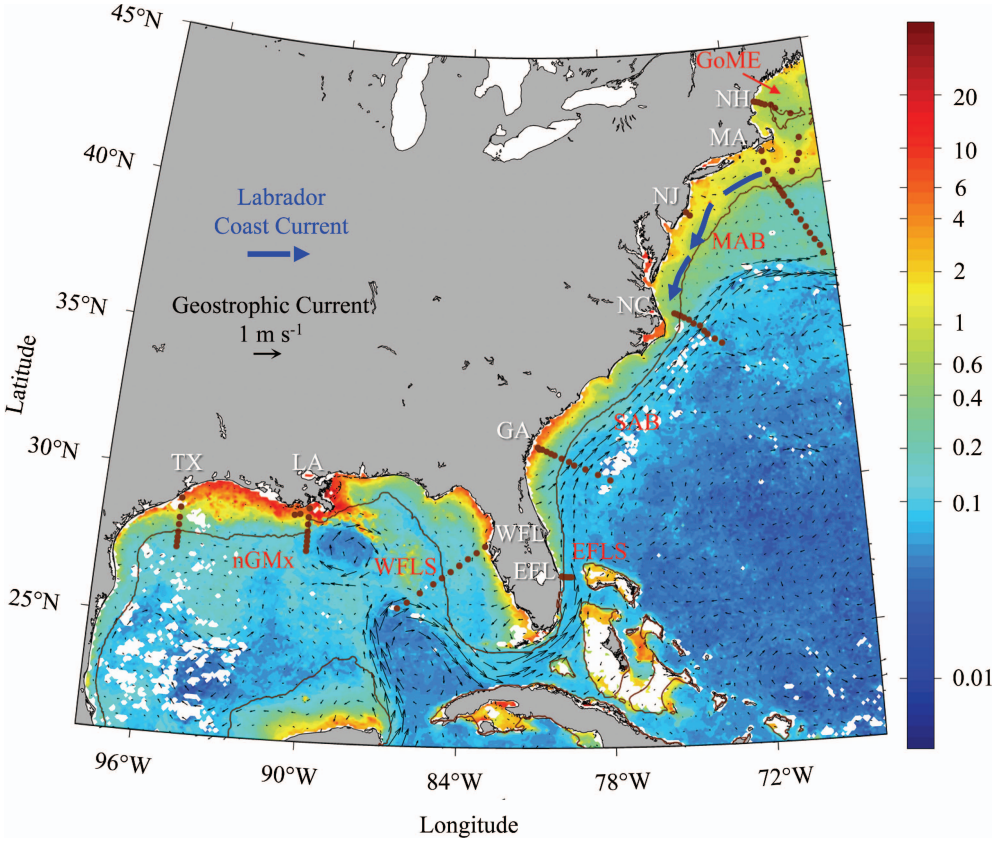

Fig. 1. Remotely sensed (SeaWiFS) sea surface chlorophyll-*a* (Chl-*a*, μg L^{-1} in color scale) and geostrophic surface current velocities (black arrows; calculated from satellite altimetry, http://www.aviso.oceanobs.com) along the U.S. Gulf of Mexico and Atlantic coasts (Jul 2007 averages). The continental shelf boundary (200 m isobath) is also shown. The six shelf regions (red lettering) are the northern Gulf of Mexico (nGMx), West Florida Shelf (WFLS), East Florida Shelf (EFLS), South Atlantic Bight (SAB), Mid-Atlantic Bight (MAB), and Gulf of Maine (GoME). The nine GOMECC hydrographic station transects, shown by the brown dots, are named according to their bordering coastal states (white lettering): Texas (TX), Louisiana (LA), West Florida (WFL), East Florida (EFL), Georgia (GA), North Carolina (NC), New Jersey (NJ), Massachusetts (MA), and New Hampshire (NH). The thick blue arrows schematically show the mean alongshore flow associated with the Labrador Coastal Current. (This current is not visible in the geostrophic current field because it is relatively weak and it is difficult for altimetric measurements to resolve the flow.)

confined to individual shelves rather than the margin as a whole. The carbonate system parameter that has been most measured along this ocean margin is the partial pressure of CO_2 (pCO_2) or CO_2 fugacity (fCO_2) in surface waters. As a result, much has been learned in recent years about air–sea CO_2 flux dynamics on seasonal to annual scales (Hales et al. 2008; Najjar et al. 2010; Wang et al. 2012). Inorganic carbon biogeochemistry and associated fluxes of constituents other than CO_2 gas are less well-known (Najjar et al. 2010; Cai 2011).

Among the U.S. Gulf of Mexico and Atlantic shelf regions, the nGMx is unique in the extent to which it is influenced by riverine input. The Mississippi–Atchafalaya River System (MARS) and numerous smaller rivers discharge high-alkalinity, high-DIC water into the enclosed subtropical gulf (Cai 2003; Keul et al. 2010). In the highly dynamic MARS plume area, high concentrations of riverine nutrients stimulate intensive biological uptake of DIC, which leads to CO_2 influx into the plume from the atmosphere over most of the year (Cai 2003; Lohrenz et al. 2010). Outside the plume, the shelf water column tends to exhibit a dominance of respiration and remineralization over primary production, and DIC values are close to those of the open gulf (Lohrenz and Cai 2006). Boundary current entrainment of shelf water occurs mainly during summer, when Loop Current eddies approach and interact with the shelf and then carry shelf water southeastward (Morey et al. 2003; Walker et al. 2005). Shelf–ocean exchange fluxes of inorganic carbon have not been well-quantified for this region (Coble et al. 2010).

On the broad WFLS, riverine influences are minimal. The ecosystem is primarily driven by microbial loop processes, and net biological uptake of DIC is limited (Wanninkhof et al. 1997; Pomeroy et al. 2000; Clark et al. 2004). Low-salinity, high-chlorophyll nGMx plume water may affect the WFLS through Loop Current entrainment

and delivery (Schiller et al. 2011). Shelf–ocean exchange of DIC for this region has not been quantified.

The narrow East Florida Shelf, which lies south of Cape Canaveral, likewise receives almost no riverine input. Shelf-specific studies of the inorganic carbon system are limited. The Florida Current frontal zone is located on the slope just off the shelf break. Upwelling events, which may occur throughout the year, are common in summer due to coastal upwelling-favorable winds (Fiechter and Mooers 2007).

The subtropical SAB is a marsh-dominated shelf (Cai et al. 2003), distinctive in that its extensive intertidal marshes are comparable to its rivers as a source of total alkalinity (TA) and organic and inorganic carbon to the shelf (Hopkinson 1988; Wang and Cai 2004). Rivers in the region are mainly small to medium in size (Menzel 1993), with relatively low DIC and TA concentrations (Wang et al. 2005). In summer and autumn, high temperatures and large marsh exports of organic and inorganic carbon favor CO_2 oversaturation and DIC loss to the atmosphere; in winter and spring, the opposite condition prevails and the system becomes a CO_2 sink (Wang et al. 2005; Jiang et al. 2008*b*). Seasonal phytoplankton blooms are not characteristic of this region, and biologically driven net DIC uptake is limited for all seasons. Sporadic blooms occur during periods of upwelling and water intrusion from the open ocean (Menzel 1993; Pomeroy et al. 2000). These events may occur throughout the year. SAB export of DIC to the open ocean has been estimated to be $\sim 2.2 \times 10^{11}$ mol C yr^{-1}, based on a mass balance model (Wang et al. 2005). Recent results from coupled circulation–biogeochemical models suggest an export flux of more than twice that (Hofmann et al. 2011).

The MAB is significantly influenced by the Labrador Coastal Current (Fig. 1), with a mean southward flow on the order of a few to 10 cm s^{-1} of low-salinity water (Beardsley and Boicourt 1981; Lentz 2008). Near Cape Hatteras, the flow turns offshore to join the Gulf Stream (Flagg et al. 2002). Total riverine inputs of inorganic carbon and alkalinity are comparable to those of the SAB (Najjar et al. 2010). MAB surface waters take up atmospheric CO_2 in the winter and spring but outgas CO_2 during summer and autumn. Winter uptake is associated with low water temperature, which increases CO_2 solubility; spring uptake coincides with phytoplankton blooms that occur when water temperatures are still relatively low (DeGrandpre et al. 2002). The MAB also experiences upwelling-triggered phytoplankton blooms (Churchill and Gawarkiewicz 2009). At the shelf edge, a strong southward jet is associated with a pronounced shelf-break front. Cross-frontal material exchange occurs throughout the MAB (Lozier and Gawarkiewicz 2001; Hales et al. 2009), and model results suggest a net annual shelf DIC export of $\sim 1.0 \times 10^{11}$ mol C yr^{-1} to the open ocean (Hofmann et al. 2011).

The semi-enclosed GoME serves as a source of water to the MAB as the major coastal current, associated with the Labrador Coastal Current, is southward (Townsend et al. 2010). Riverine concentrations and fluxes of TA and DIC in the GoME are relatively small (Cai et al. 2010; Najjar et al. 2010). The region experiences a large influx of atmospheric CO_2 associated with regular spring blooms, but this seasonal gain is offset by autumn-to-winter vertical mixing and CO_2 efflux (Salisbury et al. 2008; Vandemark et al. 2011). The GoME is partially isolated from the open Atlantic Ocean by large shallow banks, but shelf–slope water interactions occur through the deeper Northeast Channel, between Browns and Georges Banks (Townsend et al. 2010). Model results indicate that GoME DIC export rates to the ocean are similar to those estimated for the SAB (Hofmann et al. 2011).

Previous work has provided an improved understanding of carbonate system dynamics in these varied regions of the U.S. Gulf of Mexico and Atlantic coasts. However, a lack of coordinated continental-scale observational studies significantly limits our ability to assess carbon distributions and fluxes across geographic boundaries and to construct climate-relevant carbon inventories and budgets for evaluation of changes related to anthropogenic forcing. As a contribution to the U.S. North America Carbon Program and the Ocean Carbon and Biogeochemistry program, the U.S. National Oceanic and Atmospheric Administration (NOAA) conducted coastal carbon cruises along the U.S. East and West coasts in the summer of 2007. Observations showing upwelling-induced coastal ocean acidification along the U.S. West Coast are described in Feely et al. (2008). Here, we present results from the Gulf of Mexico and East Coast Carbon (GOMECC) cruise, the first to undertake comprehensive measurements of all primary inorganic carbon system parameters in these coastal waters. This paper focuses specifically on the summertime observations of TA and DIC across geographic regions characterized by a wide range of oceanographic and biogeochemical conditions. Emphasis is particularly directed to an examination of regional differences in CO_2 species and properties (e.g., aragonite saturation state, buffer intensity) and to selected case studies of contributing processes, such as alongshore mixing and biogeochemical processing (MAB), and shelf–boundary current–ocean interaction (Gulf of Mexico and southeastern shelves).

Methods

Sampling—The R/V *Ronald H. Brown* departed Galveston, Texas, on 10 July 2007 to sample waters along and across the nGMx and West Florida shelves, then exited via the Straits of Florida to continue sampling along and across shelf regions from the EFLS to the GoME. The cruise ended in Boston, Massachusetts, on 04 August 2007. A complete description of the cruise and parameters measured is provided in the NOAA cruise report (www.aoml.noaa.gov/ocd/gcc/GOMECC).

Ninety hydrographic stations were occupied along nine transects that ran approximately orthogonal to the coast (Fig. 1). Each transect is named according to its bordering coastal state: Texas (TX), Louisiana (LA), West Florida (WFL), East Florida (EFL), Georgia (GA), North Carolina (NC), New Jersey (NJ), Massachusetts (MA), and New Hampshire (NH). The EFL transect extended only to the middle of the Gulf Stream ($\sim$ 50 km offshore) due to international clearance issues. Along the NJ transect, ship

mechanical problems limited sampling to only 2 of 10 scheduled stations.

At each station, a rosette with 24 Niskin bottles and conductivity–temperature–depth (Seabird SBE 9-plus) and oxygen (Seabird SBE43) sensors was deployed. The vertical resolution of discrete sampling was ~ 20 m for water depths < 100 m, ~ 30 m for water depths between 100 m and 200 m, ~ 50 m for water depths between 200 m and 400 m, ~ 100 m for water depths between 400 m and 800 m, and ~ 200 m for water depths > 800 m. These resolutions were comparable to those of previous coastal carbon studies. Discrete water samples were collected for measurement of nutrients (nitrate, phosphate, and silicate) and carbonate parameters (TA, DIC, and fCO_2). Nutrient samples were drawn using standard containers; protocols are described in the cruise report cited above. Bottle samples for the three carbonate parameters were poisoned with saturated mercuric chloride using standard protocols described in Dickson et al. (2007).

TA, DIC, and fCO_2 *analyses*—A modified Gran titration procedure (Cai et al. 2010; Wang and Cai 2004) was used to determine the TA of discrete samples within 24 h of collection. Titrations were conducted potentiometrically with an automated titrator (AS-ALK2; Apollo SciTech) using an open-cell configuration and a ROSS™ combination electrode (Thermo Fisher Scientific) at a controlled temperature. A known volume of acid (HCl) was added to each 25 mL water sample to lower its pH to < 4.5. Small HCl increments were then added stepwise until the sample pH was < 3.0. The volume of HCl needed to lower the pH of the original sample to the pH equivalence point (pH ~ 4.5) was obtained from linear Gran Function relationships. The HCl concentration was determined by titration of Certified Reference Material (CRM) provided by Dr. A.G. Dickson at the Scripps Institution of Oceanography. The precision and accuracy of the TA measurements were determined to be better than ± 2.0 μmol kg^{-1}.

All DIC bottle measurements were made onboard the ship within 12 h of collection. DIC was measured coulometrically (Dickson et al. 2007) with an analytical system consisting of a coulometer (UIC, Inc.) coupled with a DIC Extractor (DICE) inlet system. Water samples were pumped into a calibrated volume on the DICE and then fed into an extraction chamber, where they were acidified and stripped with CO_2-free air or nitrogen gas. The purged gas was then swept into the titration cell of the coulometer for detection. The coulometer was calibrated by measurements of two calibrated volumes of pure CO_2 (99.995%) gas; the carbon masses corresponding to the gas loop volumes bracketed the range of DIC concentrations encountered in the seawater samples. CRM was used to adjust the values obtained by the coulometric system for small offsets between the CRM and coulometer values. The DIC measurements had a precision of ± 1.0 μmol kg^{-1}. The overall uncertainty, based on day-to-day offsets between reported and measured CRM values, was 2.0–3.0 μmol kg^{-1}.

Discrete fCO_2 samples were measured within 6 h of collection at a controlled temperature (20°C). Analysis of discrete fCO_2 at 20°C [fCO_2(20)] is described in Wanninkhof and Thoning (1993). Each bottle sample was CO_2-equilibrated with a known volume of headspace air that was circulated in a closed loop under temperature-controlled conditions. The CO_2 mole fraction in the equilibrated headspace air was measured with an Infra-Red analyzer (LI-COR 6262) that was calibrated using a set of six gas standards obtained from Scott-Marin; these standards were traceable to CO_2 primary standards on the World Meteorological Organization 78 scale. The results were corrected for water vapor concentration, barometric pressure, and changes created by the headspace–water mass transfer. The analysis had a precision within ± 1.0 μatm and an accuracy of ± 3.0 μatm.

Evaluation of internal consistency—Measurement of DIC, TA, fCO_2(20), and nutrient concentrations allowed assessment of the thermodynamic consistency of the shipboard carbonate system measurements. CO_2 system calculations based on the Microsoft Excel program by Pierrot et al. (2006) were performed using the carbonic acid constants of Mehrbach et al. (1973) as refitted by Dickson and Millero (1987). The fCO_2(20)–TA pair was chosen to calculate DIC (DIC_{cal}) for comparison with measured values (DIC_{mea}). Residuals between DIC_{cal} and DIC_{mea} (n = 762) were randomly distributed, indicating no systematic errors in the measurements of DIC, TA, or fCO_2(20). The mean difference between DIC_{cal} and DIC_{mea} was 1.2 (± 3.8) μmol kg^{-1} (one standard deviation, 1σ) or 0.06% (± 0.18%), well within the propagated uncertainties of the measurements (Millero 2007).

Calculation of other CO_2 *system variables*—Seawater pH on the total hydrogen ion concentration scale at 20°C, pH_T(20), was calculated using the TA–DIC pair and the software and carbonic acid constants described above. Although the fCO_2–DIC and fCO_2–TA pairs yield better calculation precision (Millero 2007), the TA–DIC pair was selected for use because (1) the GOMECC TA and DIC measurements were evaluated using CRMs (no CRMs are available for fCO_2), and (2) more measurements were available for TA (n = 973) and DIC (n = 968) than for fCO_2(20) (n = 769).

The in situ saturation state (solubility ratio) for aragonite (Ω_A) is given by

$$\Omega_A = \left[CO_3^{2-}\right] \left[Ca^{2+}\right] / K_{sp} \quad (1)$$

where $\left[CO_3^{2-}\right]$ is the carbonate ion concentration, $[Ca^{2+}]$ is the calcium ion concentration, and K_{sp} is the stoichiometric solubility product of aragonite. Carbonate ion concentrations were obtained from the TA–DIC pair, and calcium ion concentrations were estimated from salinity (S). K_{sp} was calculated as a function of in situ temperature, salinity, and pressure according to the parameterizations of Millero (1995) and Mucci (1983). Calculations of saturation state (Eq. 1) were made using either the program of Pierrot et al. (2006) or Ocean Data View (http://www.odv.awi.de); the two packages produced identical results.

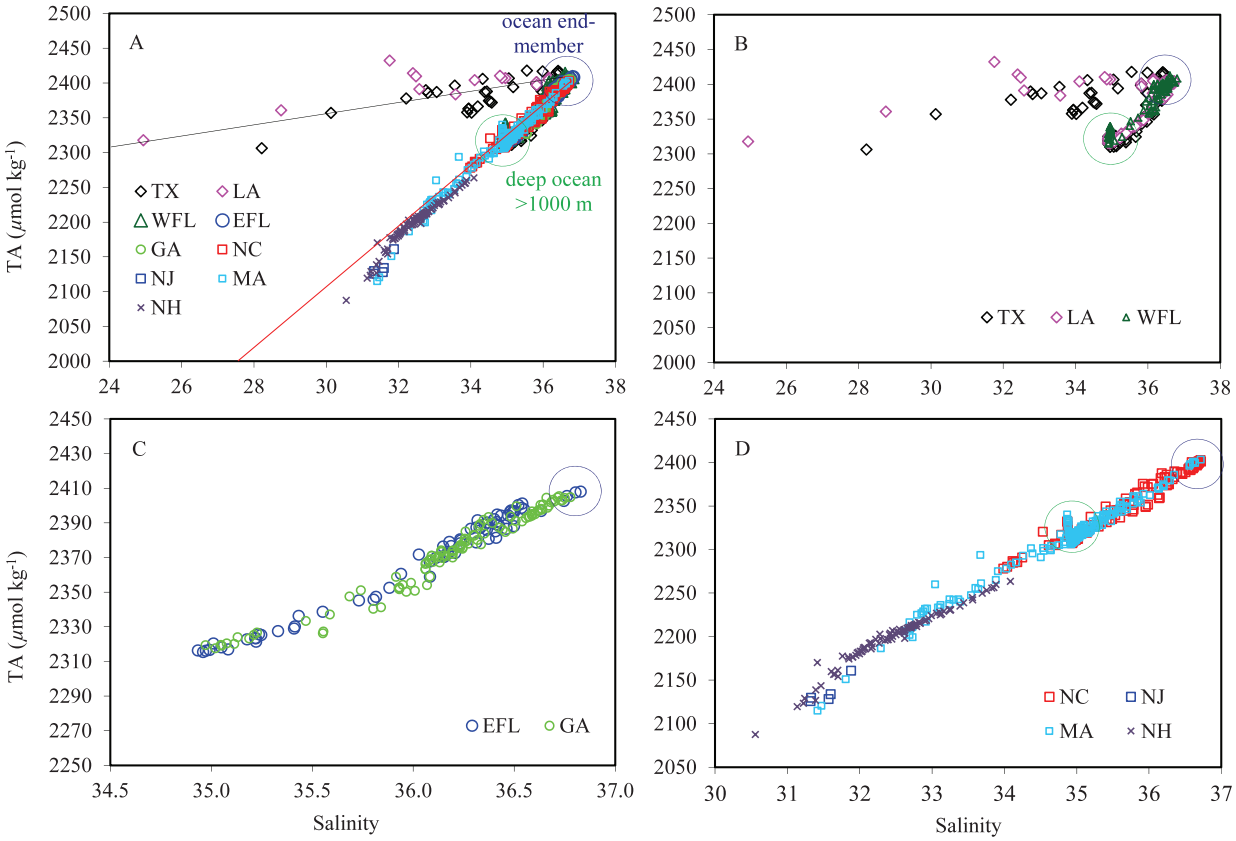

Fig. 2. TA–salinity plots for (A) all transects; (B) TX, LA, and WFL transects; (C) EFL and GA transects; and (D) NC, NJ, MA, and NH transects. The blue circles on panels A–D encompass the ocean end-member points; the green circles on panels A–B and D encompass data collected from > 1000 m depth. (The solid lines in [A] are shown for explanatory purposes; *see* text.)

Results

Hydrographic and biogeochemical conditions for surface waters along the U.S. Gulf of Mexico and Atlantic coasts during the GOMECC cruise were well-depicted in ocean color and altimetric satellite imagery (Fig. 1). Highest surface chlorophyll was seen in the plume water of the Mississippi–Atchafalaya river system. This feature, typical of the nGMx, extended far offshore. High-chlorophyll water in the other shelf regions was mainly confined to nearshore areas. In the central Gulf of Mexico, the Loop Current could be clearly seen in the July 2007 geostrophic surface current vectors (calculated from satellite altimeter data; http://www.aviso.oceanobs.com). A powerful anticyclonic ring that had earlier separated from the current was stalled in the northern gulf, spinning just east of the LA transect. A patch of high-chlorophyll water could also be seen just north of the WFL transect, likely resulting from Loop Current entrainment and southward transport of highly productive nGMx water. Along the Atlantic coast, no shelf influence from Florida Current–Gulf Stream rings was evident. At the time of the cruise, all coastal states east of Louisiana and south of New Jersey were experiencing drought conditions (Seager et al. 2009).

Total alkalinity—TA over all shelf regions behaved largely conservatively, with two dominant mixing regimes sharing a common oceanic end-member (Fig. 2A–D, blue circles). The water common to both groups was warm (mean temperature = 21.6°C) and salty (= 36.7) with high TA (= 2404 μmol kg^{-1}). This water, which constituted the core of the Loop Current–Florida Current–Gulf Stream system, occurred at a mean depth of 130 m offshore from the shelves of the LA, WFL, EFL, GA, NC, and MA transects. A tongue of deep water with salinity 34.8–35.0 and TA 2320–2340 μmol kg^{-1} (Fig. 2A,B,D, green circles) was found at deep offshore stations (> 1000 m) of the WFL, NC, and MA transects. These waters, with a TA slightly elevated compared with shelf waters of the same *S*, potentially resulted from the mixing of slope and deep oceanic waters.

Inshore stations of the TX and LA transects (Fig. 2A, black line) strongly reflected the dominating influence of riverine alkalinity inputs. The lowest salinities of the entire cruise were encountered here ($S \sim 24$–25), but the TA values ($\sim$ 2325 μmol kg^{-1} at the lowest) were only slightly depressed from oceanic values. This distinctive signal can be attributed to the high concentrations of bicarbonate ion delivered by the region's major rivers, the Mississippi (TA $\sim$ 2400 μmol kg^{-1}) and the Atchafalaya (TA $\sim$ 2000 μmol kg^{-1}; Cai et al. 2010). The scatter of the TA–*S* data points (best seen in Fig. 2B) is attributed to the region's multiple riverine sources (Mississippi vs. Atchafalaya River; Cai et al. 2010; Guo et al. 2012). The outer shelf and off-shelf waters of

the TX and LA transects fell along the more oceanic end of the lower mixing line (Fig. 2A, red line; and Fig. 2B). Waters of the Florida peninsula (WFL and EFL transects) and the GA transect similarly clustered near the oceanic end member (Fig. 2B,C).

The freshest waters of the second mixing group (Fig. 2A, red line) were encountered in the western GoME (NH transect). Two distinct line segments were seen, with the segment representing the fresher waters ($S < 31.8$) being more steeply sloped (Fig. 2D). Extrapolating this lower segment to $S = 0$ indicates a freshwater end-member of TA < 100 μmol kg^{-1}. The nearest riverine end-member (Merrimack River) has a summer TA value of ~ 350 μmol kg^{-1} (Salisbury et al. 2009), which suggests that other low-TA, low-S sources may be important. Extrapolating the upper line segment to $S = 0$ yields an intercept of TA ~ 930 μmol kg^{-1}, indicating a greater kinship to waters characteristic of the Labrador Sea to the north (Cai et al. 2010).

In the MAB (Fig. 2D), a notable difference was evident between the TA–S properties of the northern (MA) and southern (NC) transects: MA waters encompassed not only oceanic end-member values but also significantly lower TA and S, while NC waters covered only the higher half of the TA–S spectrum. Similar to NH, the MA mixing line was segmented, but with a bend at $S \sim 32.7$. Mixing effects at NC (Fig. 2D) were similar to those at the GA and EFL transects to the south (Fig. 2C).

The accompanying cross-sections (Fig. 3) show the spatial distributions of the various waters sampled. The high-S, high-TA signature of the boundary current waters ($S > 36.5$, TA ~ 2400 μmol kg^{-1}) can be seen from the nGMx to the northern MAB, with the position relative to the shelf break varying greatly (Figs. 1, 3). Along the southern coast between the WFL and GA–NC transects, the apparent cross-sectional area of this boundary current water (shown in orange in Fig. 3) increased markedly.

In the nGMx (TX and LA transects), the MARS plume appeared as a small lens of low-S, moderate-TA water on the inner shelf. Summertime westward advection of the plume (Schiller et al. 2011), from Louisiana toward Texas, was responsible for the more offshore location of the lens to the west. Outside the plume area, shelf water was stratified and contained high TA. The layer of high-S, high-TA subsurface water just off the shelf break at LA coincided with the location of the anticyclonic Loop Current eddy (Figs. 1, 3).

On the wide West Florida Shelf (WFL transect; Fig. 3) waters of uniformly high TA were encountered, with little difference between the inner and outer shelf. On the narrow East Florida Shelf (EFL transect), TA values were slightly lower and similarly lacked a strong cross-shelf gradient. These patterns are consistent with the relative lack of terrestrial input to Florida's peninsular coasts. One notable feature of the EFL section was the strong vertical TA gradient observed just seaward of the shelf break, with less alkaline, deeper slope waters separated from overlying waters. This feature also coincided with low temperatures ($< 10^{\circ}$C) and high nitrate concentrations (> 25 μmol kg^{-1}) at the bottom, suggesting an upwelling event. Such events occur here often in summer (Fiechter and Mooers 2007). Characteristic boundary current water (high-S, high-TA) was found within 30 km of the shoreline at EFL, while such waters were more than 200 km offshore at WFL.

The GA transect, in contrast to the Florida cross-sections, showed greater horizontal variation (Fig. 3), with nearshore water of relatively low TA bounded by a salinity (density) front $\sim$ 20–25 km offshore. Seaward of the front, TA was higher and relatively uniform out to the shelf break. Compared with previous studies (Cai et al. 2003; Wang et al. 2005; Jiang et al. 2008*a*), nearshore TA during the GOMECC cruise was relatively low, which may be related to the 2007 drought conditions and reduced terrestrial (marsh and riverine) TA exports to the shelf (Cai et al. 2010). Near the shelf break, Florida Current water mixed with shelf waters. For all the southernmost transects (TX, LA, WFL, EFL, and GA), deep slope waters typically had lower TA concentrations than did adjacent shelf waters.

Within the MAB, the north-to-south difference in alkalinity (Fig. 2D) is apparent in the accompanying cross-sections (Fig. 3). The MA transect exhibited not only lower TA but also a stronger cross-shelf gradient than was seen at NC, with MA alkalinity increasing ~ 200 μmol kg^{-1} between the nearshore fresher water (~ 2100 μmol kg^{-1}) and the shelf break (> 2300 μmol kg^{-1}). The well-known shelf-break front, sometimes defined by $S = 34.5$ (Linder and Gawarkiewicz 1998), was clearly evident. This seasonally migratory front is typically found at its most offshore position in June and July, when shelf waters are generally freshest. Saltier slope water of intermediate TA ($\sim$ 2300–2350 μmol kg^{-1}) separated shelf waters from the high-S, high-TA Gulf Stream water, which was much farther off the shelf break at MA ($\sim$ 270 km) than at NC ($\sim$ 70 km).

In the GoME (NH transect), low-TA surface water (~ 2100 μmol kg^{-1}) was found near shore (Merrimack River plume) and also in the central gulf (Fig. 3). The water column was strongly stratified, consistent with the gulf's semi-enclosed nature, strong summer insolation, and freshwater inputs from local rivers and the Labrador Coastal Current. TA increased with depth but never exceeded 2300 μmol kg^{-1}. At 300–400 km offshore, over the Georges Bank, the water column was more vertically uniform, with a TA value of ~ 2200 μmol kg^{-1}.

Total dissolved inorganic carbon—The DIC–salinity plot (Fig. 4A) and the nitrate–salinity plot (Fig. 4B) both showed trends indicative of significant biological control, strikingly different from the TA–salinity trends (Fig. 2). For all shelf areas, surface DIC concentrations were generally low (< 2000 μmol kg^{-1}) and nitrate concentrations were near zero, consistent with biological uptake. The lowest DIC concentrations (~ 1860 μmol kg^{-1}) were observed in nearshore surface waters of the LA transect, coincident with the MARS plume area. At high salinities, many DIC–S data points fell along an arc defined by surface, subsurface, and deep waters with a wide range of DIC concentrations ($\sim$ 2000–2200 μmol kg^{-1}) but a small range of salinity (34.9–36.7). All subsurface water in the GoME (NH transect) had high DIC and low S, which differentiated these waters from the arc-shaped continuum.

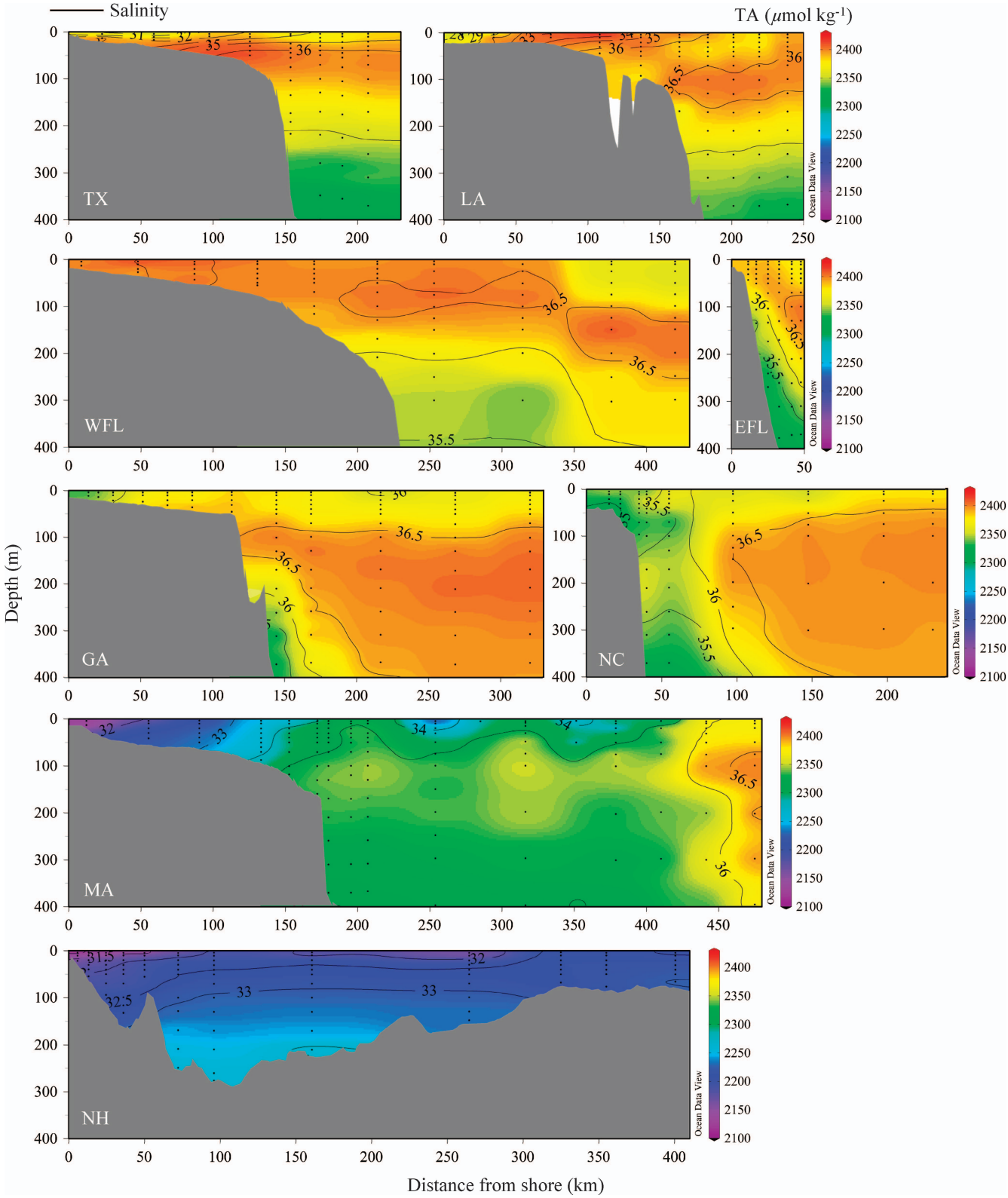

Fig. 3. Cross-shelf distributions of TA (μmol kg^{-1} in color scale) and S (contour lines) for shelf and upper slope regions. The plots were generated by Ocean Data View (http://odv.awi.de) using the VG (variable grid) gridding routine. The black dots show sample locations and depths. Transect locations are shown on Fig. 1.

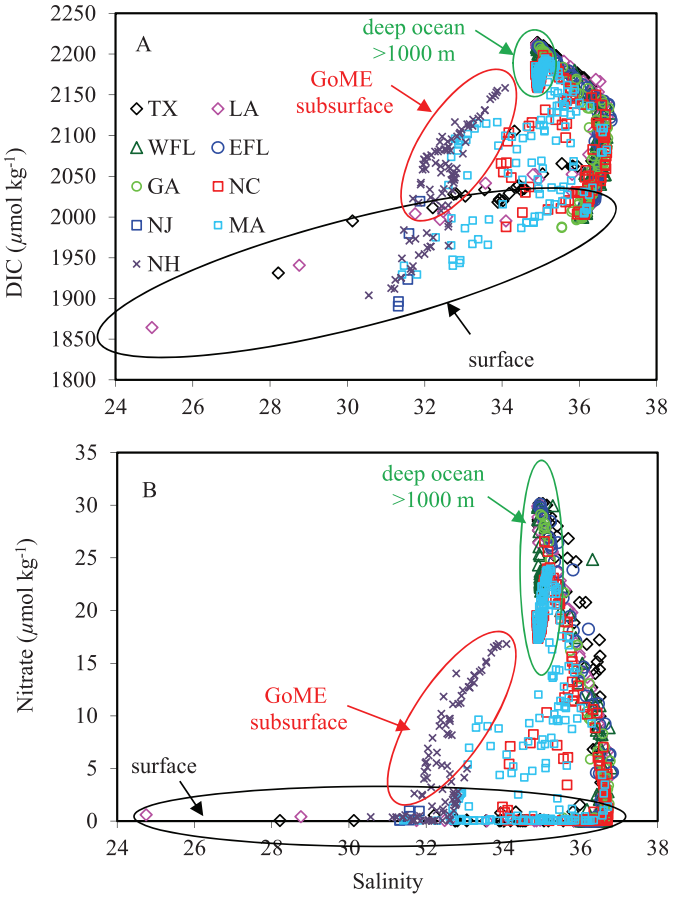

Fig. 4. Property–salinity plots for all cruise data: (A) DIC–salinity, and (B) nitrate–salinity.

A similar distribution—with a continuum of variable nitrate, high-*S* waters and distinctly different subsurface GoME waters—was seen in the nitrate–salinity plot (Fig. 4B). Intermediate in character between the distinct band of subsurface GoME water and the high-*S* continua of the southern shelves were the subsurface MAB shelf waters of the MA and NC transects (Fig 4).

In the accompanying DIC cross-sections (Fig. 5), one of the most notable differences from the TA cross-sections (Fig. 3) is the absence of an obvious boundary current signature. Surface and near-surface waters at boundary current locations (all transects from LA to MA, including the anticyclonic LA eddy) had DIC values (~ 2000–2030 μmol kg^{-1}) lower than surrounding waters. Another difference is that TA tended to decrease with depth (except in the GoME) but DIC tended to increase. This pattern of spatial variation suggests that net biological uptake of DIC dominated near the surface, while remineralization prevailed at depth. This conclusion is further supported by the distributions of nitrate (Fig. 4) and phosphate (not shown).

The distinctive low-DIC, low-*S* waters shown in Fig. 4 can be seen in the accompanying cross-sections (Fig. 5) to be associated with the river plume of the nGMx (TX and LA transects), where DIC drawdown is primarily due to enhanced primary production (Cai 2003; Lohrenz et al. 2010; Guo et al. 2012). As with TA, plume influences on DIC occurred closer to shore off Louisiana than Texas. Nearshore TX bottom water contained elevated DIC; this feature was not seen in the LA transect.

On the West Florida Shelf (WFL transect), the cross-shelf DIC gradient was small, with a range of ~ 2050–2100 μmol kg^{-1}. The East Florida Shelf (EFL transect) exhibited a strong vertical structure, with high-DIC upper-slope water (> 2200 μmol kg^{-1}) associated with the upwelling described above. The SAB (GA) transect (Fig. 5) showed a cross-shelf DIC gradient similar to that of TA (Fig. 3), with the inner-shelf density front separating nearshore low-DIC waters from mid-shelf intermediate-DIC waters.

In the MAB, the cross-shelf DIC distribution along the southern (NC) transect differed significantly from that of the northern (MA) transect (Fig. 5). On the NC shelf, little horizontal or vertical variation occurred. The water column was largely characterized by intermediate DIC concentrations (~ 2050 μmol kg^{-1}), with higher values seen in bottom waters just beyond the shelf break. Along the MA transect, however, a layer of surface water with low DIC (~ 1950 μmol kg^{-1}) extended from nearshore regions to the shelf-break front. The DIC content of most bottom water on the shelf (~ 2100 μmol kg^{-1}) was significantly higher than in the surface water. The vertical DIC gradient was more pronounced than the cross-frontal gradient, different from the pattern seen for TA (Fig. 3).

In the GoME (NH transect), low-DIC surface water was similar to that encountered at the MA transect (Fig. 5). Strong vertical gradients were observed, with deep bottom waters (> 200 m) having DIC concentrations in excess of 2150 μmol kg^{-1}. Over Georges Bank, at the outer stations of the transect, the TA and *S* data (Fig. 3) indicated a well-mixed water column, but surface waters nevertheless exhibited CO_2 undersaturation (data not shown) and DIC was significantly lower than in subsurface waters (Fig. 5). This pattern is consistent with high local biological productivity.

Discussion

The GOMECC cross-shelf observations of TA and dissolved inorganic carbon, with TA distributions closely coupled with water mass mixing and DIC bearing the overprint of biogeochemical control, showed large-scale regional differences along the U.S. Gulf of Mexico and Atlantic coasts (Figs. 2–5). These observations provide insight into the implications of regionally varying controls on CO_2 system parameter distributions. The large-scale, internally consistent data set also allows for first-order assessments of shelf–ocean interactions along the Gulf of Mexico and southeastern U.S. coasts and the interplay of physical and biogeochemical processes associated with alongshore flow in the GoME and MAB regions.

Regional differences in carbonate chemistry—The ratio of TA to dissolved inorganic carbon concentration (TA : DIC) is of particular interest because it serves as an indicator of the relative abundance of carbonate species (e.g., HCO_3^- and CO_3^{2-}) in seawater. As such, for a specific temperature and

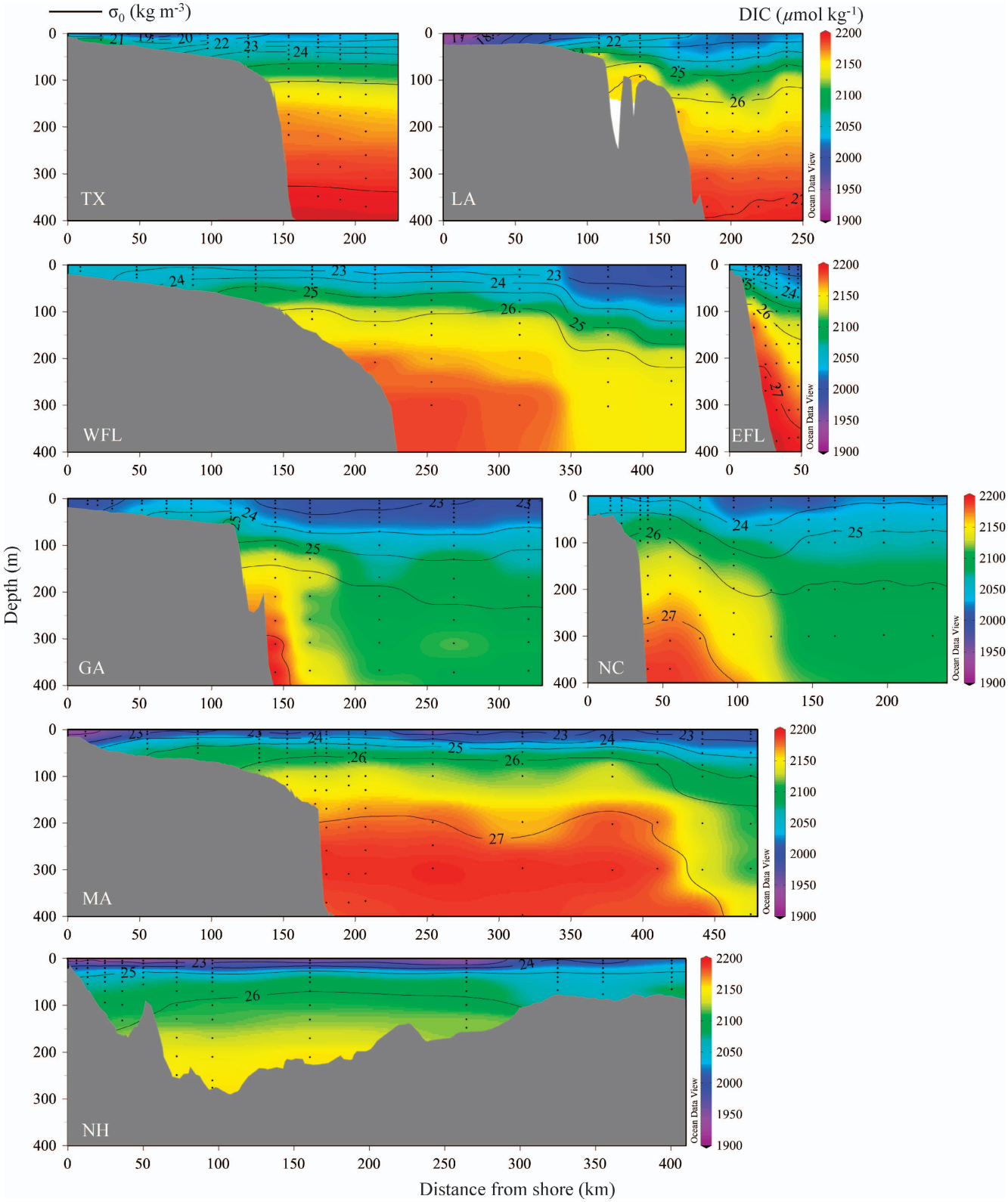

Fig. 5. Cross-shelf distributions of DIC (μmol kg^{-1} in color scale) and potential density (σ_0, kg m^{-3} in contour lines) for shelf and upper slope regions; σ_0 is referenced to surface pressure. See Fig. 3 caption for legend and plotting details. Transect locations are shown on Fig. 1.

pressure, CO_2 system parameters such as aragonite saturation state and pH are closely correlated with this ratio, which has been widely used in studies of seawater carbonate chemistry (e.g., Wanninkhof et al. 1999; Zeebe and Wolf-Gladrow 2001). The TA : DIC ratio contains information similar to the difference between TA and DIC (TA − DIC = $[CO_3^{2-}]$ − $[CO_2^*]$ + borate alkalinity + other alkalinity, where CO_2^* is the sum of dissolved CO_2 and carbonic acid [Broecker et al. 1979; Broecker and Peng 1982]). Differences in seawater TA : DIC, imply, for example, differences in buffer intensity, also called buffer capacity. The buffer intensity of the seawater carbonate system attains a minimum when $[CO_3^{2-}] \sim [CO_2^*]$, where TA and DIC concentrations are approximately equal (i.e., when TA : DIC ≈ 1). Under this condition, the Revelle factor and other buffer factors that quantitatively express the degree of buffering of CO_2, pH, and calcium carbonate ($CaCO_3$) saturation states with respect to changes in TA and DIC also reach a minimum (Egleston et al. 2010). Changing TA : DIC provides a direct mechanism for altering the sensitivity of seawater pH, Ω_A, and other CO_2-related properties to carbonate system perturbations.

For the transects sampled by the GOMECC cruise, TA : DIC ratios (Fig. 6) were greatest on the inner LA transect (~ 1.24), in association with high Mississippi–Atchafalaya riverine input of TA and intensive biological uptake of DIC in the plume waters. Ratios were lowest in the bottom waters of the NH transect (~ 1.04), reflecting the semi-enclosed nature of the GoME and the accumulation of remineralization products at depth. For all transects, TA : DIC generally decreased with depth. Cross-sectional and vertical gradients of TA : DIC were especially weak for WFL and GA shelf waters, with values being generally high (1.12–1.17). Spatial gradients were relatively well-developed on other shelves. The GOMECC TA : DIC cross-sections also illustrate that along the U.S. Gulf of Mexico and Atlantic coasts in summer 2007, the most buffered waters were encountered just off the LA coast and the least buffered were found in the deep GoME.

Isolines of aragonite saturation state, Ω_A, closely followed contours of TA : DIC (Fig. 6), as expected. The relationship was one of direct (though not strictly linear) proportionality: where TA : DIC was high, so was aragonite saturation state. All shelf and upper slope waters sampled by GOMECC were supersaturated with respect to aragonite ($\Omega_A > 1$). Shelf values of Ω_A on the southern transects (~ 2.5–4.0) were generally higher than those to the north. Inner LA waters were distinctive, with $\Omega_A > 5.0$. NH bottom waters had the lowest values, with $\Omega_A < 1.3$. Relatively low saturation states ($\Omega_A < 2$) were also found in much of the shelf water sampled along the MA transect. The close correspondence between TA : DIC and Ω_A is apparent in Eq. 1 and Fig. 7: $[CO_3^{2-}]$ and TA : DIC are tightly positively correlated, both on- and off-shelf. This close correspondence arises from the definitions of TA and DIC; it is not unique to the GOMECC data set. Cross-sectional distributions of $pH_T(20)$ (not shown) were also very similar to those of TA : DIC, with shelf values ranging from ~ 8.5 (LA surface waters) to 7.7 (deep GoME).

Large-scale regional differences in the carbonate chemistry of shelf waters can be summarized in terms of the shelf means of various parameters (Fig. 8). For the NH transect, all sampled waters were considered to be shelf samples. Elsewhere, shelf waters were defined as those encountered shoreward of the 200 m isobath. (Using the 100 m or 300 m isobath as the shelf–slope boundary produced no significant difference from the means and variances shown in Fig. 8.) Average shelf TA (Fig. 8A) was nearly constant for the three Gulf of Mexico transects (~ 2390 μmol kg^{-1}) and was just slightly lower at EFL and GA. Between the SAB and the GoME, mean shelf TA declined progressively northward, with a total decrease of ~ 170 μmol kg^{-1}. Mean shelf DIC, in contrast, hovered near ~ 2150 μmol kg^{-1} (Fig. 8A); the range for transect means was 2031 to 2082 μmol kg^{-1}. The greatest deviation from this typical mean DIC was seen on the narrow EFLS, where high-DIC slope water intruded shoreward of the 200 m isobath (Fig. 5).

For TA : DIC (Fig. 8B), mean shelf values were generally highest for the southern transects (TX, LA, WFL, and GA): TA : DIC ~ 1.17. At EFL, the mean ratio was slightly lower (~ 1.14) due to the aforementioned high DIC values. North of the GA transect, mean shelf TA : DIC fell steadily, reaching a GOMECC-wide low of 1.07 in the GoME. The strong semi-quantitative predictive power of TA : DIC can be seen in the extent to which mean $pH_T(20)$ and $fCO_2(20)$ follow this ratio. (To isolate the effects of chemical composition from the effects of temperature, Fig. 8B shows pH and fCO_2 at a fixed temperature and pressure rather than in situ conditions.) The relationship to CO_2 fugacity is an inverse one: when TA : DIC is high, $fCO_2(20)$ is low, making conditions more favorable for oceanic uptake of atmospheric CO_2.

TA and DIC concentrations are independent of temperature, but in situ pH, fCO_2, and Ω_A are not: lowering seawater temperature tends to increase pH and substantially decrease fCO_2 while moderately lowering Ω_A. The close correspondence between the trends in TA : DIC and Ω_A (Figs. 6, 8C) suggests that regional differences in shelf mean saturation state were driven largely by concentration changes and not by temperature. As an example of the extent to which lower temperatures might have contributed to lower Ω_A on the more northerly shelves, consider a parcel of average (shelf mean) nGMx seawater (TA = 2394 μmol kg^{-1}, DIC = 2047 μmol kg^{-1}, S = 33, and t = 28°C). Cooling that water by 17°C (the extent to which mean shelf temperature decreased between the two regions; Fig. 8D) lowers Ω_A by ~ 0.35, or only ~ 15% of the total observed change. In other words, most of the difference in Ω_A between the nGMx and the GoME was due to differences in chemical composition and not temperature.

Differences in TA : DIC (buffer intensity) and differences in physical conditions (temperature and salinity) are relevant to considerations of how seawater acidity ($[H^+]$) may respond to coastal acidification, such as may accompany increases in atmospheric CO_2 or eutrophication events (Cai et al. 2011). Again consider a parcel of average (shelf mean) nGMx seawater, which Fig. 8 shows to be relatively well-buffered (TA = 2394 μmol kg^{-1}, DIC = 2047 μmol kg^{-1},

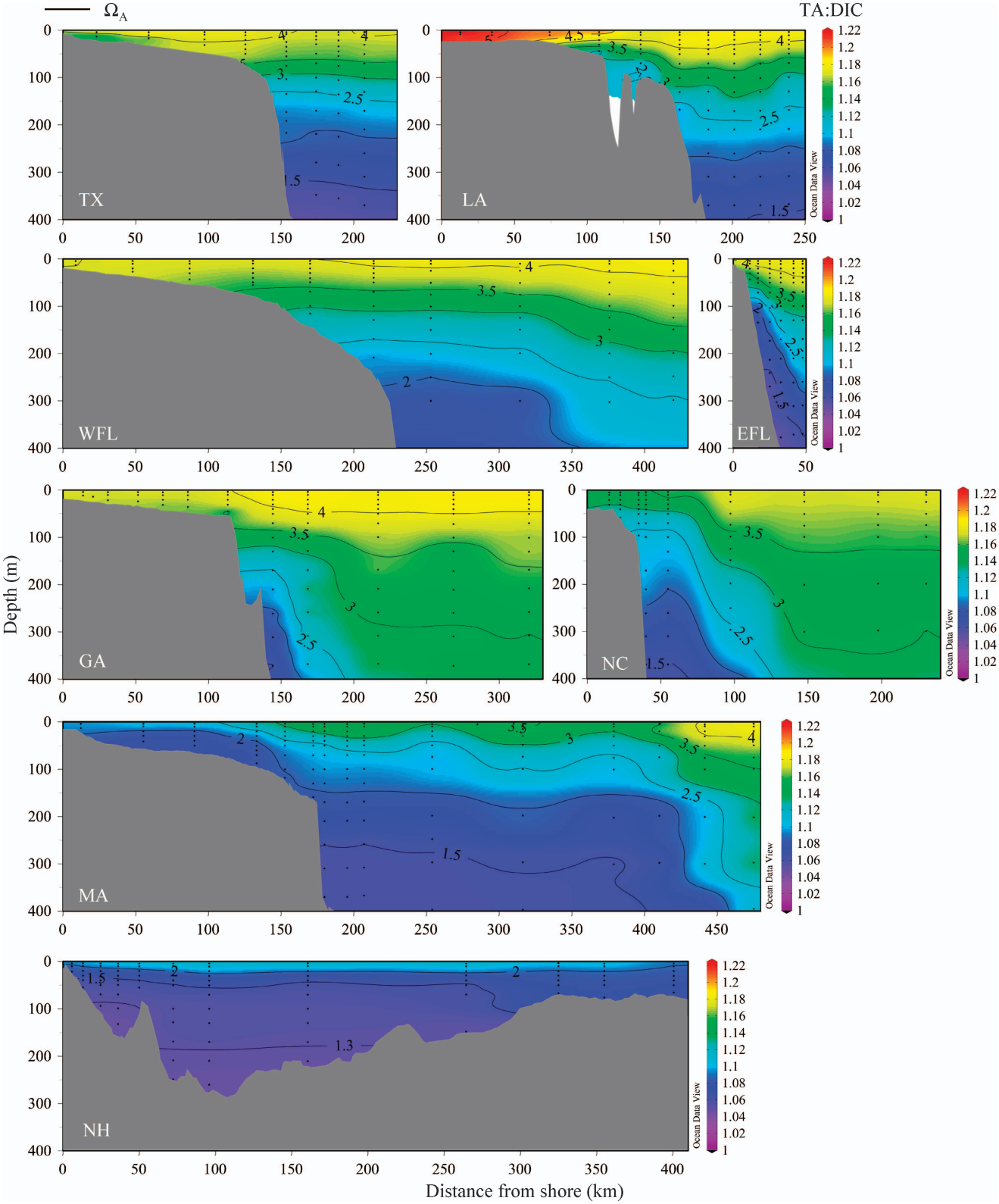

Fig. 6. Cross-shelf distributions of TA : DIC (in color scale) and calculated in situ aragonite saturation state (Ω_A, contour lines) for shelf and upper slope regions. See Fig. 3 caption for legend and plotting details. Transect locations are shown in Fig. 1.

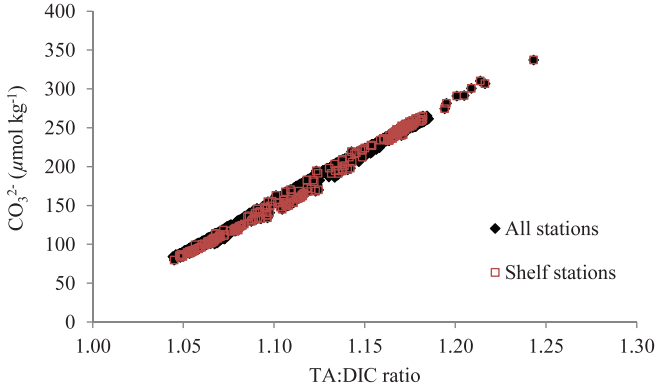

Fig. 7. Carbonate ion (CO_3^{2-}) concentrations (calculated) and TA : DIC (measured) for all GOMECC data.

TA : DIC = 1.17; fCO_2 = 371 μatm, phosphate = 0.07 μmol kg^{-1}, silicate = 2.5 μmol kg^{-1}, S = 33, and t = 28°C). For every 1 μatm increase of seawater fCO_2, [H$^+$] increases by 1.8 × 10^{-5} μmol kg^{-1}. Now consider a parcel of average (shelf mean) GoME seawater (TA = 2199 μmol kg^{-1}, DIC = 2047 μmol kg^{-1}, TA : DIC 1.07; fCO_2 = 434 μatm, phosphate = 0.7 μmol kg^{-1}, silicate = 6.1 μmol kg^{-1}, S = 32, and t = 11°C). The same 1 μatm increase in seawater fCO_2 now results in an [H$^+$] increase of 2.0 × 10^{-5} μmol kg^{-1}, 11% greater than for the nGMx water. Comparing the same two water parcels but at a single temperature (e.g., 11°C) indicates that nearly a third of the 11% difference in [H$^+$] increase can be attributed solely to differences in TA : DIC. The remaining signal is due to the difference in temperature (i.e., CO_2 solubility); salinity has a minimal effect. In other words, GoME shelf-water acidity is more responsive to changing seawater fCO_2 than is the case for an nGMx water parcel. The low buffer intensity of northeastern U.S. shelf waters suggests that such waters are more susceptible to acidification pressures and will reach critical ecological thresholds (e.g., Ω_A = 1, or higher saturation states in some cases; Barton et al. 2012) more quickly than waters along the southeastern coast and Gulf of Mexico.

Alongshore mixing and biogeochemical processing along the northeastern U.S. coast—The design of the GOMECC sampling program and the differing behaviors of TA and DIC made it possible to estimate the relative effects of physical mixing and biogeochemical processing on DIC distributions between the GoME and the southern MAB. For a first-order estimate of the effects of alongshore physical mixing, we took account of the fact that the MAB receives much of its water from the north across the Georges Bank (near the NH transect), and most of the equatorward flow turns offshore near Cape Hatteras (near the NC transect [Beardsley and Boicourt 1981; Lozier and Gawarkiewicz 2001; Lentz 2008]). We also assume that the system is at steady state and that physical and biogeochemical conditions in the MAB and GoME did not change over the transit time of the equatorward flow (a few months). Given that TA behaved largely conservatively (Fig. 2A), the observed NH-to-NC downstream increase in TA and salinity (ΔTA = 132 μmol kg^{-1} and ΔS = 3; Fig. 8) can be largely attributed to the mixing of shelf and slope waters in association with the mean southward flow. Using a mean TA : DIC ratio of 1.088 as a conversion factor (calculated from all NH, MA, and NC shelf data; 1σ = ± 0.032) yields an estimated equivalent ΔDIC of 120 μmol kg^{-1}. This value gives the mixing-induced downstream increase in DIC that would be expected had DIC behaved conservatively.

Biogeochemical processes such as photosynthesis, respiration, and air–sea CO_2 exchange also change the DIC

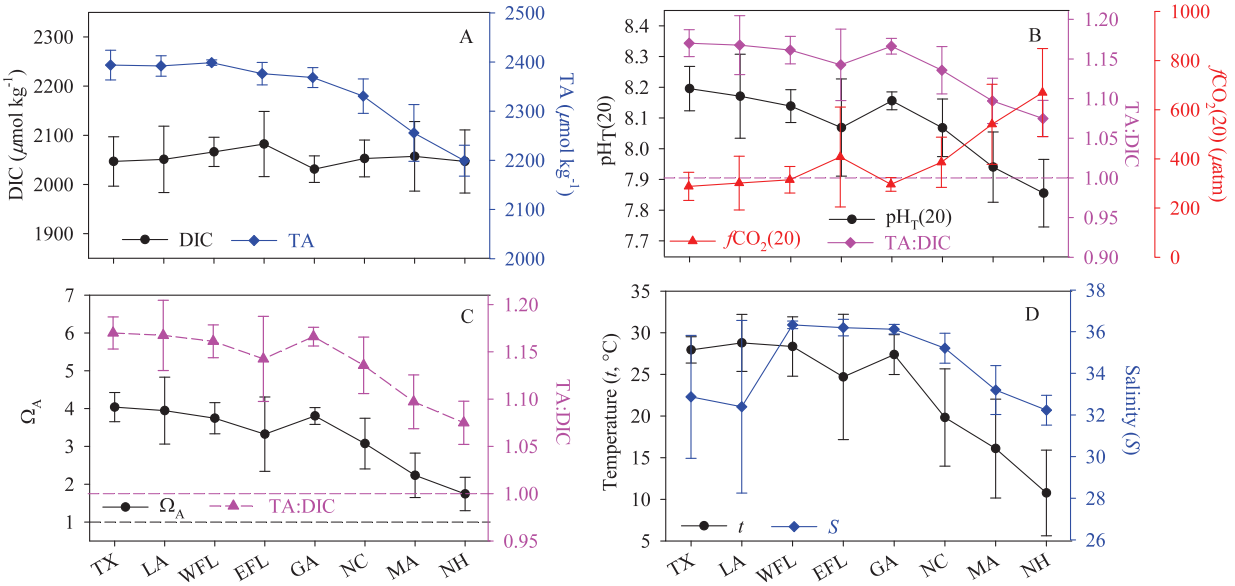

Fig. 8. Transect means for shelf samples: (A) DIC and TA; (B) TA : DIC, pH_T(20), and fCO_2(20); (C) TA : DIC and aragonite saturation state, Ω_A; and (D) temperature (t) and salinity (S). Vertical bars denote one standard deviation. Data from the NJ transect are not shown because only two stations were sampled, both on the inner shelf.

content of the water as it travels southward. To estimate the effect of these nonconservative processes, we calculated the change in salinity-normalized DIC (enDIC) for each shelf-water sample between the NH and NC transects (Friis et al. 2003):

$$\mathrm{enDIC} = \left(\mathrm{DIC_{spl}} - \mathrm{DIC}_{S=0}\right)/S \times S_{\mathrm{ref}} + \mathrm{DIC}_{S=0} \quad (2)$$

where $\mathrm{DIC_{spl}}$ is the DIC concentration measured in the sample; $\mathrm{DIC}_{S=0}$ is the DIC concentration of the freshwater end member, determined as given in Cai et al. (2010), including the assumption that DIC $\approx$ TA in river waters (Table 1); S is the salinity of the sample; and S_{ref} is the reference salinity (35) to which DIC is normalized. The downstream change in mean shelf-water enDIC between NH and NC was thus estimated to be -86 μmol kg^{-1} (Table 1). The implication is that biogeochemical processes unrelated to salinity differences (i.e., processes other than shelf mixing) are responsible for this apparent southward loss of DIC. This is consistent with previous reports of MAB net ecosystem production of total organic carbon (5.4–6.9 mol C m^{-2} yr^{-1}; Biscaye and Anderson 1994; Vlahos et al. 2002), which suggests net biological contribution to the enDIC decrease. The GOMECC observations also showed oversaturation of MAB surface seawater fCO_2 with respect to the atmospheric level (i.e., CO_2 outgassing, which would also decrease enDIC).

These first-order estimates suggest that, in the MAB, the downstream effects of physical mixing (+120 μmol kg^{-1}) and nonconservative processes (-86 μmol kg^{-1}) on shelf-water DIC were of roughly the same magnitude but opposing sign. This finding is consistent with the GOMECC observations of a small net difference in mean shelf DIC between the NH and NC transects (+6 μmol kg^{-1}; Fig. 8A and Table 1).

Shelf–boundary current–ocean interactions along the southern U.S. coasts—Directly assessing shelf–ocean carbon exchange is difficult due to the complexity of biogeochemical and physical processes near and across shelf breaks (Liu et al. 2010; Najjar et al. 2010). The GOMECC data set and the differing behaviors of TA and DIC made possible a first-order assessment of shelf–ocean exchange for the Gulf of Mexico and southern U.S. Atlantic shelves. The TA data (Figs. 2, 3) suggest that the Loop Current–Florida Current–Gulf Stream system interacted directly with shelf waters in these regions. The DIC data (Fig. 4) indicate that boundary current DIC concentrations varied along the flow path.

The Gulf Stream system can be viewed as a 'conveyer belt' that continuously interacts with surrounding waters over a time scale of days to weeks. Chemical changes along the way may occur due to endogenous processes (e.g., respiration or other forms of biogeochemical processing within the boundary current waters) and exogenous processes (i.e., through mixing and entrainment of shelf or open-ocean waters with different chemical properties). Both types of processes likely occur to variable extents along the flow path. For this analysis, the Gulf Stream system's 'initial' state upon entry into the Gulf of Mexico was characterized using previously published data, and downstream TA and DIC changes were tracked using the GOMECC data.

Table 1. Dissolved inorganic carbon (DIC) concentrations and salinities of northeastern U.S. shelf waters. Salinity-normalized DIC (enDIC) was calculated according to Eq. 2. DIC and enDIC concentrations are in μmol kg^{-1}.

	NC transect	MA transect	NH transect
Mean shelf-water salinity	35.2	33.2	32.2
Freshwater end-member DIC*	671	809	933
Mean shelf-water DIC	2053	2057	2047
Mean shelf-water enDIC	2047	2108	2133
Change in enDIC between NH and NC transects	—	—	−86

* From Cai et al. (2010).

Information about the TA and DIC content of the source water feeding the Loop Current was taken from a number of sources. According to a NOAA Coral Reef Watch ocean acidification model (Gledhill et al. 2008), waters entering the Gulf of Mexico through the Yucatan Channel before and during the GOMECC cruise had mean TA $\sim$ 2400 μmol kg^{-1} and mean DIC $\sim$ 2039 μmol kg^{-1} (model results were normalized to S = 36.7 to match boundary current salinity). Field observations near Puerto Rico in September 2006 documented subsurface Caribbean Sea water with physical properties (z = 75 m, S = 36.6, and potential density σ_0 = 24.2 kg m^{-3}) similar to those of the Gulf Stream; for these waters, DIC = 2043 μmol kg^{-1} (Wang and Byrne 2010). Field observations north of the Yucatan Channel in July 2010, along the path of the incoming Loop Current, documented surface water with TA = 2387 μmol kg^{-1}, DIC = 2036 μmol kg^{-1}, and S = 36.5 (R. Wanninkhof, http://www.aoml.noaa.gov/ocd/gcc/shortcruises/NancyFoster_2010); normalizing these values to the mean salinity of Gulf Stream water (S = 36.7) yields TA = 2397 μmol kg^{-1} and DIC = 2044 μmol kg^{-1}. Averaging over all three data sets yields an estimated TA of 2399 μmol kg^{-1} and DIC of 2042 μmol kg^{-1} for Loop Current source waters (Fig. 9A,B, green squares).

Boundary current water was identified within the GOMECC data set based on literature characterizations of Gulf Stream 'core' salinity and σ_0 values (Leaman et al. 1989; Schmitz 1996): S = 36.5–36.7, σ_0 = 24.5–26.5 kg m^{-3}, and depth $<$ 500 m. To minimize the signal from surface processes (e.g., air–sea exchange and photosynthesis), near-surface ($<$ 70 m) data were excluded. This current core, which accounts for $>$ 40% of the Gulf Stream transport volume along this margin (Leaman et al. 1989), had temperatures between 18°C and 25°C in the GOMECC data. Figure 9 shows boundary current chemical and physical properties at the GOMECC transects. At the outer WFL stations, where we sampled the Loop Current proper (Fig. 1), mean core-water TA = 2404 μmol kg^{-1} and DIC = 2107 μmol kg^{-1} (Fig. 9A,B). The difference between the source-water concentrations and these values suggests that as the Loop Current meandered through the

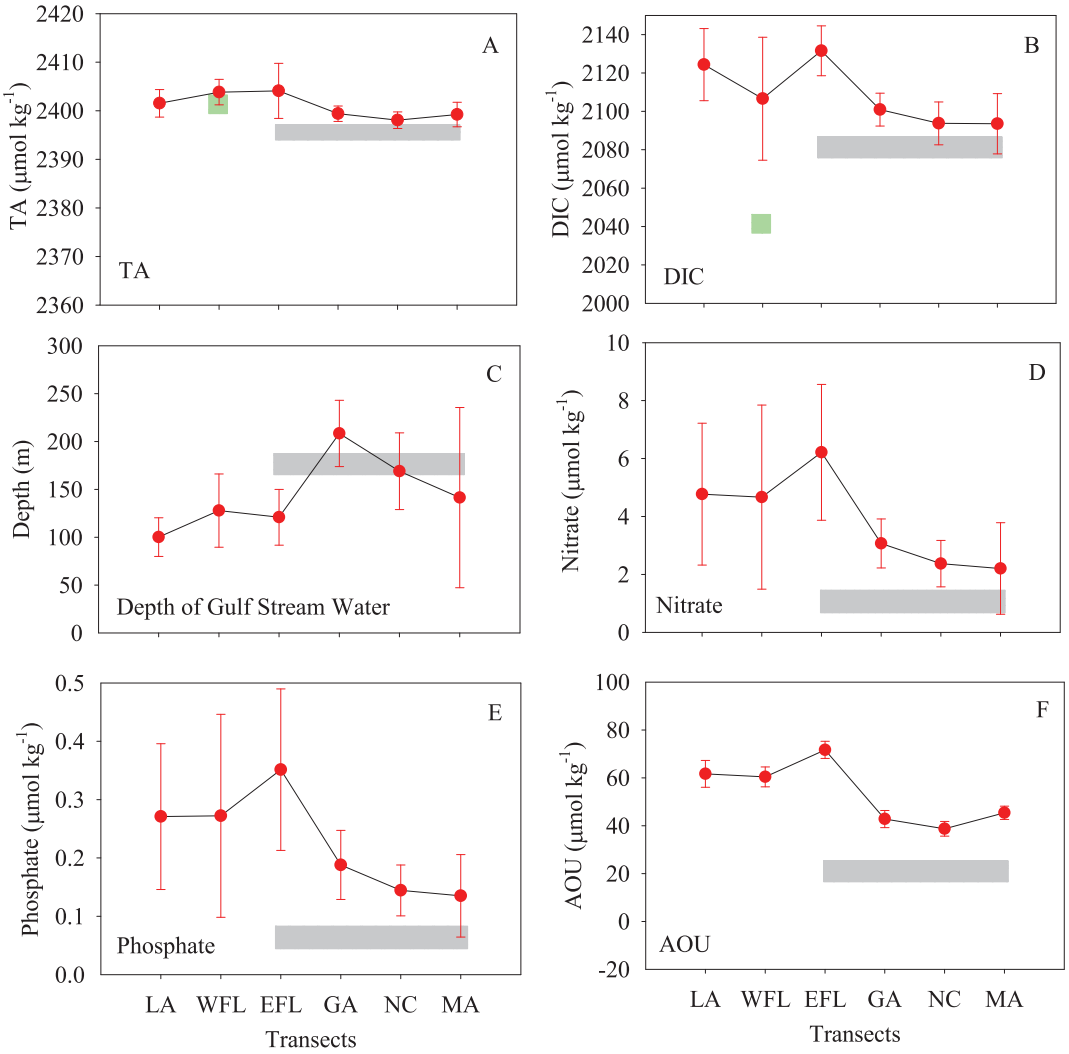

Fig. 9. Boundary current core-water means: (A) TA; (B) DIC; (C) depth; (D) nitrate; (E) phosphate; and (F) apparent oxygen utilization, AOU. The vertical bars represent 95% confidence intervals. The green-shaded squares indicate the TA and DIC content of the Loop Current source water (mean values and 95% CIs). The gray-shaded areas show parameter values (means and 95% CIs) for central Sargasso Sea Water with σ_0 values similar to those of the Gulf Stream (24.5–26.5 kg m^{-3}; CLIVAR A22, Nov 2003; http://cdiac.ornl.gov/).

gulf, from the Yucatan entrance to the WFLS, its waters experienced no appreciable TA change but a DIC increase on the order of 65 μmol kg^{-1}.

What processes might be responsible for this apparent increase in DIC concentration? The neglible change in mean TA suggests that net $CaCO_3$ dissolution or precipitation was not likely responsible, because this process increases TA and DIC in a 2 : 1 ratio. The effects of air–sea CO_2 exchange have been intentionally excluded by confining the analysis to subsurface core water (mean depth 100–130 m in the GMx; Fig. 9C), which was below the mixing-layer depth observed for the open gulf during the cruise ($\sim$ 75 m). Moreover, if the mean CO_2 flux of $\sim$ 1.8 mmol m^{-2} d^{-1} calculated for the WFL shelf (www.aoml.noaa.gov/ocd/gcc/GOMECC) is taken as representative of upstream conditions, then air–sea CO_2 exchange during the Loop Current transit time of $\sim$ 12 d would have decreased mixing layer DIC by $<$ 0.5 μmol kg^{-1}. (The transit-time estimate is based on a distance of $\sim$ 880 km between the GMx entrance and WFL, and a July 2007 mean current velocity of 0.8 m s^{-1}; Hybrid Coordinate Ocean Model, http://hycom.org.) As a first-order estimate, the effects of photosynthesis, which decreases seawater DIC, may also be excluded. The core water under consideration was deeper than the typical base of the GMx euphotic zone, which ranges from $\sim$ 4 m in highly productive plume waters to $\sim$ 82 m in oligotrophic blue waters (Lee et al. 2007).

Community respiration could have contributed to a DIC increase below the euphotic zone. Direct measurements of respiration in the gulf are lacking (Coble et al. 2010), but on the outer shelves of the SAB, where marsh carbon exports have a limited effect and the Gulf Stream exerts some influence, a mean summertime community respiration rate of 1.8 ($\pm$ 0.8) mmol C m^{-3} d^{-1} has been measured (Jiang et al. 2010). We assumed a similar community respiration rate in the Loop Current. Given the estimated transit time of $\sim$ 12 d, the DIC increase within the Loop Current due to

endogenous respiration between the GMx entrance and WFL would be ~ 23 μmol kg^{-1}, or ~ 35% of the estimated total.

DIC-rich waters from outside the current core likely contributed the remaining 65%. Vertical mixing would have been limited by strong stratification of the water column, as evidenced by σ_0 distributions at the WFL open gulf stations (Fig. 5). Gulf and shelf waters adjacent to the Loop Current had relatively high DIC (e.g., WFL transect; Fig. 5) and constitute plausible sources of boundary current DIC supply. The 12 d Loop Current transit time suggests a net DIC contribution of 3.5 mmol m^{-3} d^{-1}. Using a mean water transport of 30 Sv (30 $\times 10^6$ m^3 s^{-1}; Schmitz 1996), this rate translates to a DIC flux of ~ 9.1 $\times$ 10^9 mol C d^{-1} (~ 3.3 $\times$ 10^{12} mol C yr^{-1}) into the Loop Current between the Yucatan Channel and the WFLS. For comparison, consider that the Mississippi–Atchafalaya river system has a DIC flux of ~ 1.8 $\times$ 10^{12} mol C yr^{-1} (Cai 2003), about one-half the above DIC flux. The fact that much of the gulf water adjacent to the Loop Current interacts directly with nearby shelves (Morey et al. 2003; Walker et al. 2005; Fig. 1) suggests that the Loop Current DIC influx was largely derived ultimately from surrounding shelf regions. Considering the fact that the MARS DIC flux peaks in spring (Cai 2003) and that other riverine and shelf processes (e.g., respiration of organic carbon) likely contributed DIC as well, the estimated rate of entrainment of shelf DIC into the Loop Current (potentially a lower-bound estimate of the total shelf DIC export) seems reasonable.

Entrainment of shelf water into the Loop Current has been best studied in the nGMx and WFLS regions, through observational, modeling, and remote sensing efforts (Hu et al. 2005; Walker et al. 2005; Schiller et al. 2011). When the current impinges against the northern shelf break, shelf–current interaction facilitates the entrainment of shelf and river-plume water, which can then be transported to the WFLS and beyond (Morey et al. 2003; Walker et al. 2005). Satellite observations of surface chlorophyll during the GOMECC cruise (Fig. 1) showed that filaments of high-chlorophyll water, apparently originating from the river outflows and then steered around an anticyclonic ring, reached the shelf break of the WFLS. Underway fCO_2 measurements during the cruise (www.aoml.noaa.gov/ocd/gcc/GOMECC) also showed surface undersaturation near the filaments of high-chlorophyll water at the WFL transect.

A similar analysis of downstream change in boundary current carbonate chemistry can be applied to the Florida Current, between the EFLS and Cape Hatteras. A complicating factor in this region is the incorporation of oligotrophic Sargasso Sea water (SSW) into the northward-flowing current. North Atlantic subtropical recirculation contributes to significant western boundary current intensification, with the transport volume increasing approximately three-fold from 30 Sv to 90 Sv between the Straits of Florida and Cape Hatteras (Schmitz 1996). This intensification is also indicated by the significant increase in the apparent cross-sectional area of the high-*S*, high-TA boundary current core water between the WFL and GA–NC transects (Fig. 3).

At the upstream end of this current segment (EFL), mean core-water TA = 2404 μmol kg^{-1} and DIC = 2132 μmol kg^{-1} (Fig. 9A,B). At the downstream (NC) end, mean TA differed very little from that initial value (ΔTA ~ -7 μmol kg^{-1}), but mean DIC was lower by ~ 40 μmol kg^{-1}. For Sargasso Sea water with a σ_0 signature similar to that of the boundary current core, mean TA and mean DIC were 2395 and 2085 μmol kg^{-1}, respectively (data from CLIVAR A22 Nov 2003, http://cdiac.ornl.gov). A 1 : 2 mixing ratio, as suggested by the northward increase in transport volume, would decrease core-water TA by ~ 6 μmol kg^{-1} and DIC by ~ 32 μmol kg^{-1}, resulting in final mean concentrations of TA ~ 2398 μmol kg^{-1} and DIC ~ 2100 μmol kg^{-1}. These values are within the 95% confidence intervals for concentrations observed at the NC transect, where mean core-water TA = 2398 ($\pm$ 2) μmol kg^{-1} and mean DIC = 2094 ($\pm$ 10) μmol kg^{-1}. Similar calculations for nitrate, phosphate, and apparent oxygen utilization indicate that incorporation of oligotrophic Sargasso Sea water can also explain most of the decrease observed in each of these quantities (Fig. 9D–F).

Calcium carbonate precipitation–dissolution likely had little effect on the change in DIC concentration over this current segment (a ΔTA of ~ -7 μmol kg^{-1} would imply a ΔDIC of ~ -3.5 μmol kg^{-1}). The effects of air–sea CO_2 exchange and photosynthesis were likely insignificant, because the Florida Current core water was deeper (mean depths 100–200 m; Fig. 9C) than the mixing layer (< 75 m deep) and the euphotic zone (< 100 m deep). We estimate that respiration would have contributed a DIC increase of ~ 10 μmol kg^{-1}, based on an EFL-to-NC transit time of ~ 10 d and a mixing-adjusted summer respiration rate of ~ 1.0 μmol C kg^{-1} d^{-1} (based on a summer SAB outer shelf mean respiration rate of 1.8 μmol C kg^{-1} d^{-1} and a summer SSW mean rate of 0.8 μmol C kg^{-1} d^{-1}; Obernosterer et al. 2003; Jiang et al. 2010). Applying both mixing and small endogenous (i.e., respiration and $CaCO_3$ precipitation) effects to the EFL boundary-current core water produces an estimated mean DIC concentration of ~ 2107 μmol kg^{-1}, which is within the 99% confidence interval for the NC observations (2094 $\pm$ 16 μmol kg^{-1}).

The rate of net DIC export from the SAB shelf has been estimated as 2.2–5.6 $\times$ 10^{11} mol C yr^{-1} (Cai et al. 2003; Wang et al. 2005; Hofmann et al. 2011). Given the flow parameters above, this level of SAB export would increase the mean boundary current core-water DIC concentration by < 2.0 μmol kg^{-1}. These calculations suggest that although SAB inorganic carbon shelf exports may be important, the effect of the contribution to boundary current DIC is masked by dilution associated with the incorporation of low-DIC SSW.

Near Cape Hatteras, the Gulf Stream is deflected into the North Atlantic, and by the latitude of the MA transect, it flows some 400 km offshore (Fig. 3). The boundary current's core-water DIC, nutrient, and O_2 concentrations at the MA transect were indistinguishable from those at NC (Fig. 9), implying that either significant entrainment of

oligotrophic water had not occurred or other processes had balanced the entrainment effect along this northern limb of the Gulf Stream system.

Implications for future studies—Large-scale coastal surveys such as the GOMECC cruise offer a means to acquire high-quality spatial (horizontal and vertical) data coverage, and they constitute an integral part of a comprehensive coastal ocean observing system. Such studies facilitate the identification and assessment of large-scale physical and biogeochemical processes that control carbon fluxes, regional inventories, and spatial gradients. The GOMECC data, unique in their transregional extent, allow us to compare and contrast, for the first time, large-scale differences in the cross-shelf distributions of all carbonate system parameters. The data also enable us to make first-order estimates of the effects of some understudied regional-scale processes, such as alongshore mixing and processing and shelf–ocean exchange. These observational studies can significantly contribute to hypothesis generation and the refinement of observational and modeling strategies to examine controlling mechanisms and more accurately constrain accompanying fluxes. For example, the boundary-current tracking method presented in this study may be further developed to improve estimates of shelf–ocean fluxes of carbon and other constituents.

The GOMECC observations also establish baseline concentration fields against which other observations, including those associated with full-scale station reoccupations such as GOMMEC-2 in 2012, can be compared. Long-term observations suitable for elucidating seasonal and interannual variabilities associated with the coastal inorganic carbon system are especially needed. In light of the prospects for future seawater acidification in coastal oceans—whether through atmospheric CO_2 accumulation, coastal eutrophication, or other ocean margin processes—systematic studies in regions such as the northeastern U.S. coast, where aragonite saturation states are at present minimally supersaturated, will be particularly important. Such undertakings are essential in assessing the effects of natural and anthropogenic changes and anticipating their probable consequences along continental margins.

Acknowledgments

We thank the officers and crew of the National Oceanic and Atmospheric Administration (NOAA) ship *Ronald H. Brown* and the participants of the 2007 Gulf of Mexico and East Coast Carbon (GOMECC) cruise (http://www.aoml.noaa.gov/ocd/gcc/GOMECC/participants.html). We thank T. Clayton for insightful editorial assistance. We also express gratitude to Burke Hales and an anonymous reviewer for their substantial and constructive reviews.

The study was supported by the NOAA Global Carbon Cycle Program, proposal GC05-208.

References

Barton, A., B. Hales, G. G. Waldbusser, C. Langdon, and R. Feely. 2012. The Pacific oyster, *Crassostrea gigas,* shows negative correlation to naturally elevated carbon dioxide levels: Implications for near-term ocean acidification effects. Limnol. Oceanogr. **57:** 698–710, doi:10.4319/lo.2012.57.3.0698

Bates, N. R., and J. T. Mathis. 2009. The Arctic Ocean marine carbon cycle: evaluation of air-sea CO_2 exchanges, ocean acidification impacts and potential feedbacks. Biogeosciences **6:** 2433–2459, doi:10.5194/bg-6-2433-2009

Beardsley, R. C., and W. C. Boicourt. 1981. On estuarine and continental shelf circulation in the Middle Atlantic Bight, p. 198–233. *In* B. A. Warren and C. Wunsch [eds.], Evolution of physical oceanography. MIT Press.

Biscaye, P. E., and R. F. Anderson. 1994. Fluxes of particulate matter on the slope of the southern Middle Atlantic Bight—seep-II. Deep-Sea Res. Part II **41:** 459–509.

Bouillon, S., and others. 2008. Mangrove production and carbon sinks: A revision of global budget estimates. Glob. Biogeochem. Cycles **22:** GB2013, doi:10.1029/2007GB003052

Broecker, W. S., and T. H. Peng. 1982. Tracers in the sea. Eldigio Press.

———, T. Takahashi, H. J. Simpson, and T. H. Peng. 1979. Fate of fossil-fuel carbon-dioxide and the global carbon budget. Science **206:** 409–418, doi:10.1126/science.206.4417.409

Cai, W.-J. 2003. Riverine inorganic carbon flux and rate of biological uptake in the Mississippi River plume. Geophys. Res. Lett. **30:** 1032, doi:10.1029/2002GL016312

———. 2011. Estuarine and coastal ocean carbon paradox: CO_2 sinks or sites of terrestrial carbon incineration? Annu. Rev. Mar. Sci. **3:** 123–145, doi:10.1146/annurev-marine-120709-142723

———, X. Hu, W.-J. Huang, L. Q. Jiang, Y. C. Wang, T. H. Peng, and X. Zhang. 2010. Alkalinity distribution in the western North Atlantic Ocean margins. J. Geophys. Res. Oceans **115:** C08014, doi:10.1029/2009JC005482

———, and others. 2011. Acidification of subsurface coastal waters enhanced by eutrophication. Natl. Geosci. **4:** 10.1038/ngeo1297.

———, Z. A. Wang, and Y. C. Wang. 2003. The role of marsh-dominated heterotrophic continental margins in transport of CO_2 between the atmosphere, the land–sea interface and the ocean. Geophys. Res. Lett. **30:** 1849, doi:10.1029/2003GL017633

Chen, C. T. A., and A. V. Borges. 2009. Reconciling opposing views on carbon cycling in the coastal ocean: Continental shelves as sinks and near-shore ecosystems as sources of atmospheric CO_2. Deep-Sea Res. Part II **56:** 578–590, doi:10.1016/j.dsr2.2009.01.001

Churchill, J. H., and G. Gawarkiewicz. 2009. Shelfbreak frontal eddies over the continental slope north of Cape Hatteras. J. Geophys. Res. Oceans **114:** C02017, doi:10.1029/2007JC004642

Clark, C. D., and others. 2004. CDOM distribution and CO_2 production on the Southwest Florida Shelf. Mar. Chem. **89:** 145–167, doi:10.1016/j.marchem.2004.02.011

Coble, P. G., L. L. Robbins, L. D. Kendra, W.-J. Cai, K. Fennel, and S. E. Lohrenz. 2010. A preliminary carbon budget for the Gulf of Mexico. Ocean Carbon Biogeochem News **3:** 1–4.

DeGrandpre, M. D., G. J. Olbu, and C. M. Beatty. 2002. Air–sea CO_2 fluxes on the US Middle Atlantic Bight. Deep-Sea Res. Part II **49:** 4355–4367, doi:10.1016/S0967-0645(02)00122-4

Dickson, A. G., and F. J. Millero. 1987. A comparison of the equilibrium constants for the dissociation of carbonic acid in seawater media. Deep-Sea Res. **34:** 1733–1743.

———, C. L. Sabine, and J. R. Christian. 2007. Guide to best practices for ocean CO_2 measurements. PICES Special Publication.

Egleston, E. S., C. L. Sabine, and F. M. M. Morel. 2010. Revelle revisited: Buffer factors that quantify the response of ocean chemistry to changes in DIC and alkalinity. Glob. Biogeochem. Cycles **24:** GB1002, doi:10.1029/2008GB003407

Feely, R. A., C. L. Sabine, J. M. Hernandez-Ayon, D. Ianson, and B. Hales. 2008. Evidence for upwelling of corrosive "acidified" water onto the continental shelf. Science **320:** 1490–1492, doi:10.1126/science.1155676

Fiechter, J., and C. N. K. Mooers. 2007. Primary production associated with the Florida Current along the East Florida Shelf: Weekly to seasonal variability from mesoscale-resolution biophysical simulations. J. Geophys. Res. Oceans **112:** C12002, doi:10.1029/2006JC003576

Flagg, C. N., L. J. Pietrafesa, and G. L. Weatherly. 2002. Springtime hydrography of the southern Middle Atlantic Bight and the onset of seasonal stratification. Deep-Sea Res. Part II **49:** 4297–4329, doi:10.1016/S0967-0645(02)00121-2

Friis, K., A. Kortzinger, and D. W. R. Wallace. 2003. The salinity normalization of marine inorganic carbon chemistry data. Geophys. Res. Lett. **30:** 1085, doi:10.1029/2002GL015898

Gledhill, D. K., R. Wanninkhof, F. J. Millero, and M. Eakin. 2008. Ocean acidification of the Greater Caribbean Region 1996–2006. J. Geophys. Res. Oceans **113:** C10031, doi:10.1029/2007JC004629

Guo, X. H., and others. 2012. Carbon dynamics and community production in the Mississippi River plume. Limnol. Oceanogr. **57:** 1–17, doi:10.4319/lo.2012.57.1.0001

Hales, B., W. J. Cai, B. Mitchell, C. Sabine, and O. Schofield. 2008. Introduction and background, p. 3–13. *In* B. Hales, W.-J. Cai, B. Mitchell, C. Sabine, and O. Schofield [eds.], North American Continental Margins: A synthesis and planning workshop. Report of the North American Continental Margins Working Group for the U.S. Carbon Cycle Scientific Group and Interagency Working Group. Washington, D.C.: U.S. Carbon Cycles Science Program. Available from http://www.us-ocb.org/publications/reports.html

———, R. D. Vaillancourt, L. Prieto, J. Marra, R. Houghton, and D. Hebert. 2009. High-resolution surveys of the biogeochemistry of the New England shelfbreak front during Summer, 2002. J. Mar. Syst. **78:** 426–441, doi:10.1016/j.jmarsys.2008.11.024

Hauri, C., N. Gruber, G. K. Plattner, S. Alin, R. A. Feely, B. Hales, and P. A. Wheeler. 2009. Ocean acidification in the California Current System. Oceanography **22:** 60–71, doi:10.5670/oceanog.2009.97

Hofmann, E. E., and others. 2011. Modeling the dynamics of continental shelf carbon. Annu. Rev. Mar. Sci. **3:** 93–122, doi:10.1146/annurev-marine-120709-142740

Hopkinson, C. S. 1988. Patterns of organic carbon exchange between coastal ecosystems—the mass balance approach in salt marsh ecosystems, p. 122–154. *In* B.-O. Jansson [ed.], Coastal-Offshore Ecosystem Interactions. Lecture Notes on Coastal and Estuarine Studies. Springer.

———, and E. M. Smith. 2005. Estuarine respiration: An overview of benthic, pelagic, and whole system respiration, p. 122–147. *In* P. del Giorgio and P. Williams [eds.], Respiration in Aquatic Ecosystems. Oxford Univ. Press.

Hu, C. M., J. R. Nelson, E. Johns, Z. Q. Chen, R. H. Weisberg, and F. E. Muller-Karger. 2005. Mississippi River water in the Florida Straits and in the Gulf Stream off Georgia in summer 2004. Geophys. Res. Lett. **32:** L14606, doi:10.1029/2005GL022942

Jiang, L. Q., W. J. Cai, and Y. C. Wang. 2008*a*. A comparative study of carbon dioxide degassing in river- and marine-dominated estuaries. Limnol. Oceanogr. **53:** 2603–2615, doi:10.4319/lo.2008.53.6.2603

———, ———, ———, J. Diaz, P. L. Yager, and X. P. Hu. 2010. Pelagic community respiration on the continental shelf off Georgia, USA. Biogeochemistry **98:** 101–113, doi:10.1007/s10533-009-9379-8

———, ———, R. Wanninkhof, Y. C. Wang, and H. Luger. 2008*b*. Air–sea CO_2 fluxes on the US South Atlantic Bight: Spatial and seasonal variability. J. Geophys. Res. Oceans **113:** C07019, doi:10.1029/2007JC004366

Keul, N., J. W. Morse, R. Wanninkhof, D. K. Gledhill, and T. S. Bianchi. 2010. Carbonate chemistry dynamics of surface waters in the northern Gulf of Mexico. Aquat. Geochem. **16:** 337–351, doi:10.1007/s10498-010-9091-2

Leaman, K. D., E. Johns, and T. Rossby. 1989. The average distribution of volume transport and potential vorticity with temperature at three sections across the Gulf Stream. J. Phys. Oceanogr. **19:** 36–51, doi:10.1175/1520-0485(1989)019<0036:TADOVT>2.0.CO;2

Lee, Z. P., A. Weidemann, J. C. Kindle, R. Arnone, K. L. Carder, and C. Davis. 2007. Euphotic zone depth: Its derivation and implication to ocean-color remote sensing. J. Geophys. Res. Oceans **112:** C03009, doi:10.1029/2006JC003802

Lentz, S. J. 2008. Observations and a model of the mean circulation over the Middle Atlantic Bight continental shelf. J. Phys. Oceanogr. **38:** 1203–1221, doi:10.1175/2007JPO3768.1

Linder, C. A., and G. Gawarkiewicz. 1998. A climatology of the shelfbreak front in the Middle Atlantic Bight. J. Geophys. Res. Oceans **103:** 18405–18423, doi:10.1029/98JC01438

Liu, K.-K., L. Atkinson, R. Quinones, and L. Talaue-McManus. 2010. Biogeochemistry of continental margins in a global context, p. 3–24. *In* K.-K. Liu, L. Atkinson, R. Quinones, and L. Talaue-McManus [eds.], Carbon and Nutrient Fluxes in Continental Margins: A Global Synthesis. Springer.

Lohrenz, S. E., and W. J. Cai. 2006. Satellite ocean color assessment of air–sea fluxes of CO_2 in a river-dominated coastal margin. Geophys. Res. Lett. **33:** L01601, doi:10.1029/2005GL023942

———, ———, F. Z. Chen, X. G. Chen, and M. Tuel. 2010. Seasonal variability in air–sea fluxes of CO_2 in a river-influenced coastal margin. J. Geophys. Res. Oceans **115:** C10034, doi:10.1029/2009JC005608

Lozier, M. S., and G. Gawarkiewicz. 2001. Cross-frontal exchange in the Middle Atlantic Bight as evidenced by surface drifters. J. Phys. Oceanogr. **31:** 2498–2510, doi:10.1175/1520-0485(2001)031<2498:CFEITM>2.0.CO;2

Mehrbach, C., C. H. Culberson, J. E. Hawley, and R. M. Pytkowicz. 1973. Measurement of apparent dissociation constants of carbonic acid in seawater at atmospheric pressure. Limnol. Oceanogr. **18:** 897–907, doi:10.4319/lo.1973.18.6.0897

Menzel, D. W. 1993. Ocean Processes: U.S. Southeast Continental Shelf. U.S. Department of Energy. Report DOEIOSTI 11674.

Millero, F. J. 1995. Thermodynamics of the carbon-dioxide system in the Oceans. Geochim. Cosmochim. Acta **59:** 661–677, doi:10.1016/0016-7037(94)00354-O

———. 2007. The marine inorganic carbon cycle. Chem. Rev. **107:** 308–341, doi:10.1021/cr0503557

Morey, S. L., W. W. Schroeder, J. J. O'Brien, and J. Zavala-Hidalgo. 2003. The annual cycle of riverine influence in the eastern Gulf of Mexico basin. Geophys. Res. Lett. **30:** 1867, doi:10.1029/2003GL017348

Mucci, A. 1983. The solubility of calcite and aragonite in seawater at various salinities, temperatures, and one atmosphere total pressure. Am. J. Sci. **283:** 780–799, doi:10.2475/ajs.283.7.780

Najjar, R., and others. 2010. Carbon budget for the continental shelf of the eastern united states: A preliminary synthesis. Ocean Carbon Biogeochem. News **3:** 1–4.

Obernosterer, I., N. Kawasaki, and R. Benner. 2003. P-limitation of respiration in the Sargasso Sea and uncoupling of bacteria from P-regeneration in size-fractionation experiments. Aquat. Microb. Ecol. **32:** 229–237, doi:10.3354/ame032229

Pierrot, D., E. Lewis, and D. W. R. Wallace. 2006. MS Excel program developed for CO_2 system calculations. Carbon Dioxide Information Analysis Center, Oak Ridge National

Laboratory. Oak Ridge, Tennessee. ORNL/CDIAC-105a, U. S. Department of Energy, doi:10.3334/CDIAC/otg.CO2SYS_XLS_CDIAC105a

Pomeroy, L. R., J. E. Sheldon, W. M. Sheldon, J. O. Blanton, J. Amft, and F. Peters. 2000. Seasonal changes in microbial processes in estuarine and continental shelf waters of the south-eastern USA. Estuar. Coast. Shelf Sci. **51:** 415–428, doi:10.1006/ecss.2000.0690

Salisbury, J., and others. 2009. Episodic riverine influence on surface DIC in the coastal Gulf of Maine. Estuar Coast Shelf S **82:** 108–118, doi:10.1016/j.ecss.2008.12.021

———, D. Vandemark, C. W. Hunt, J. W. Campbell, W. R. McGillis, and W. H. McDowell. 2008. Seasonal observations of surface waters in two Gulf of Maine estuary-plume systems: Relationships between watershed attributes, optical measurements and surface pCO_2. Estuar. Coast. Shelf Sci. **77:** 245–252, doi:10.1016/j.ecss.2007.09.033

Schiller, R. V., V. H. Kourafalou, P. Hogan, and N. D. Walker. 2011. The dynamics of the Mississippi River plume: Impact of topography, wind and offshore forcing on the fate of plume waters. J. Geophys. Res. Oceans **116:** C06029, doi:10.1029/2010JC006883

Schmitz, W. J. 1996. Some global features / North Atlantic circulation. On the world ocean circulation, v. 1. Woods Hole (MA): Woods Hole Oceanographic Institution. Tech. Rept. WHOI-96-03.

Seager, R., A. Tzanova, and J. Nakamura. 2009. Drought in the southeastern United States: Causes, variability over the last millennium, and the potential for future hydroclimate change. J. Clim. **22:** 5021–5045, doi:10.1175/2009JCLI2683.1

Takahashi, T., and others. 2009. Climatological mean and decadal change in surface ocean pCO_2, and net sea–air CO_2 flux over the global oceans. Deep-Sea Res. Part II **56:** 554–577, doi:10.1016/j.dsr2.2008.12.009

Thomas, H., Y. Bozec, and K. Elkalay. 2004. Enhanced open ocean storage of CO_2 from shelf sea pumping. Science **304:** 1005–1008, doi:10.1126/science.1095491

Townsend, D. W., N. D. Rebuck, M. A. Thomas, L. Karp-Boss, and R. M. Gettings. 2010. A changing nutrient regime in the Gulf of Maine. Cont. Shelf Res. **30:** 820–832, doi:10.1016/j.csr.2010.01.019

Tsunogai, S., S. Watanabe, and T. Sato. 1999. Is there a "continental shelf pump" for the absorption of atmospheric CO_2? Tellus **51B:** 701–712, doi:10.1034/j.1600-0889.1999.t01-2-00010.x–712

Vandemark, D., and others. 2011. Temporal and spatial dynamics of CO_2 air–sea flux in the Gulf of Maine. J. Geophys. Res. Oceans **116:** C01012, doi:10.1029/2010JC006408

Vlahos, P., R. F. Chen, and D. J. Repeta. 2002. Dissolved organic carbon in the Mid-Atlantic Bight. Deep-Sea Res. Part II **49:** 4369–4385, doi:10.1016/S0967-0645(02)00167-4

Walker, N. D., W. J. Wiseman, L. J. Rouse, and A. Babin. 2005. Effects of river discharge, wind stress, and slope eddies on circulation and the satellite-observed structure of the Mississippi River plume. J. Coast. Res. **21:** 1228–1244, doi:10.2112/04-0347.1

Wang, Z. A., and R. H. Byrne. 2010. Summer-time CO_2 fluxes and carbonate system behavior in the Mississippi River and Orinoco River Plumes. *In* J. Hall, D. E. Harrison, and D. Stammer [eds.], OceanObs'09, 21–25 September 2009. Proceedings of OceanObs'09: Sustained Ocean Observations and Information for Society (Annex). ESA Publication WPP-306, doi:10.5270/OceanObs09

———, and others. 2012. Air–sea exchange, p. 10–11. *In* R. G. Najjar, M. Friedrichs, and W.-J. Cai [eds.], Gloucester Point (VA): Report of the U.S. East Coast Carbon Cycle Synthesis Workshop, Available from http://www.us-ocb.org/publications/reports.html.

———, and W.-J. Cai. 2004. Carbon dioxide degassing and inorganic carbon export from a marsh-dominated estuary (the Duplin River): A marsh CO_2 pump. Limnol. Oceanogr. **49:** 341–354, doi:10.4319/lo.2004.49.2.0341

———, ———, Y. C. Wang, and H. W. Ji. 2005. The southeastern continental shelf of the United States as an atmospheric CO_2 source and an exporter of inorganic carbon to the ocean. Cont. Shelf Res. **25:** 1917–1941, doi:10.1016/j.csr.2005.04.004

Wanninkhof, R., and others. 1997. Gas exchange, dispersion, and biological productivity on the West Florida Shelf: Results from a Lagrangian tracer study. Geophys. Res. Lett. **24:** 1767–1770, doi:10.1029/97GL01757

———, E. Lewis, R. A. Feely, and F. J. Millero. 1999. The optimal carbonate dissociation constants for determining surface water pCO_2 from alkalinity and total inorganic carbon. Mar. Chem. **65:** 291–301, doi:10.1016/S0304-4203(99)00021-3

———, and K. Thoning. 1993. Measurement of fugacity of CO_2 in surface-water using continuous and discrete sampling methods. Mar. Chem. **44:** 189–204, doi:10.1016/0304-4203(93)90202-Y

Zeebe, R. E., and D. Wolf-Gladrow. 2001. CO_2 in seawater—equilibrium, kinetics, isotopes. Elsevier.

Associate editor: Markus H. Huettel

Received: 11 June 2012
Accepted: 20 August 2012
Amended: 20 October 2012